MARCH 2025

The Epicenter of Geophysical Excellence

GSH Journal

GEOPHYSICAL SOCIETY OF HOUSTON
Volume 1 • Number 1

Technical Articles:

TABLE *of* CONTENTS

MEETINGS

FEATURES

On The Cover...

The graphic on the front represents the results of a self-organizing map (SOM), one of the machine learning processes in the Paradise® software by Geophysical Insights. Each hexagon is a neuron corresponding to a data cluster from a multi-attribute classification done in attribute space and then mapped to a 2-D colormap for dimensionality reduction and analysis.

Image courtesy of Geophysical Insights

LOOK INSIDE

CHECK THIS OUT

EDITOR'S NOTE

To ensure inclusion in the Journal, please note that information, advertisements, and articles need to be submitted at least 8 weeks in advance of publication. Submit your articles and any questions to Paul Schatz, Editor at pschatz@everestcognition.com. Thanks to the editorial team:

Editor	***Paul Schatz***
Technical Articles	***Scott Singleton***
	Alvaro Chaveste
Doodlebugger Diary	***Scott Singleton***
Museum	***Bill Gafford***

GEOPHYSICAL SOCIETY OF HOUSTON ORGANIZATION CONTACTS

Kathy Sanvido: Office Manager and Webmaster
1790 W. Sam Houston Parkway N., Houston, TX 77043
Phone: (281) 741-1624 • Email: office@gshtx.org • Website: http://www.gshtx.org

		Email
PRESIDENT	**Mihai Popovici**	mihai@z-terra.com
Sponsorship		
PRESIDENT ELECT	**Rene Mott**	queenmio@att.net
GSH MEMBERSHIP		
PAST PRESIDENT	**Katie Baker**	katiebaker.gsh@gmail.com
PRIOR PAST PRESIDENT	**Peter Eick**	peter.eick@gmail.com
TECHNICAL EVENTS		
FIRST VICE PRESIDENT	**Wilson Ibanez**	wibanez@slb.com
FIRST VICE PRESIDENT ELECT	**Kurang Mehta**	kurangmehta.geophysics2022@gmail.com
Tech Luncheons	Wilson Ibanez	wibanez@slb.com
Continuing Education / Webinars	Mike Graul	mgraul@texseis.com
Spring Symposium	Wilson Ibanez	wibanez@slb.com
Fall Forum	Wilson Ibanez	wibanez@slb.com
SPECIAL INTEREST GROUPS (SIGS)		
Data Processing and Acquisition	Carlos Espinoza	cespinoza@slb.com
Data Science and Machine Learning	Erkan Ay	erkan.ay@shell.com
Potential Fields	John Greene	john.greene@chevron.com
Rock Physics	Sue Pritchett	spritchett@ikonscience.com
Unconventional	Scott Singleton	Scott.Singleton@comcast.net
Unconventional & New Energy	Scott Singleton	Scott.Singleton@comcast.net
SOCIAL / FUNDRAISING EVENTS		
SECOND VICE PRESIDENT	**Marie Clavaud**	marie.clavaud@tgs.com
SECOND VICE PRESIDENT ELECT	**Paul Vincent**	pvincent@chevron.com
NextGen	Casey Ruplinger	caseyrup46@gmail.com
Warm Up Shoot	John Asma	johna@z-terra.com
Icebreaker	Marie Clavaud	marie.clavaud@tgs.com
Salt Water Fishing Tournament	Nathan Lenz	nathaniel.lenz@tgs.com
Pickleball Tournament	Russell Jones	newrjones1@yahoo.com
Sporting Clays	John Asma	johna@z-terra.com
Golf Tournament	Denise Dorsey	ddorsey@ikonscience.com
Annual Meeting & Awards Banquet	Rene' Mott	queenmio@att.net
Axe Throwing	Casey Ruplinger	caseyrup46@gmail.com
FINANCE		
TREASURER	**Troy Hawkes**	thawkes@chevron.com
TREASURER-ELECT	**Arpita Bathija**	apal_b@yahoo.com
Finance Committee	K Rene' Mott	queenmio@att.net
RECORDS		
SECRETARY	**Whitney Schultz**	whitneyschultz.gsh@gmail.com
COMMUNICATION DIRECTOR	**Liza Yellott**	lyellott@ikonscience.com
COMMUNICATION DIRECTOR-ELECT	**Cucha Lopez**	cc.lopezr@gmail.com
Commercial Tech Events - GDTB	Liza Yellott	lyellott@ikonscience.com
Editor	Paul Schatz	PSchatzwrk@gmail.com
Website	Paul Schatz	PSchatzwrk@gmail.com
Social Media Lead	Liza Yellott	lyellott@ikonscience.com
SEG SECTION REPRESENTATIVES	**Patrick Corwin**	patrick_corwin@oxy.com
Katie Baker		katiebaker.gsh@gmail.com
Mihai Popovici		mihai@z-terra.com
SEG ALTERNATE REPS	**Lee Lawyer**	llawyer@prodigy.net
Allen Bertagne		abertagne@comcast.net
OUTREACH		
Outreach K-12	Sara Tirado	outreach@gshtx.org
Scholarship Liaison	Patrick Corwin	patrick_corwin@oxy.com
GEOSCIENCE CENTER	**Bill Gafford**	geogaf@hal-pc.org
Historian	Bill Gafford	geogaf@hal-pc.org
ECH liaison	Katya Casey	katya.casey@actusveritas.com
ECH liaison	Huw James	huwejames@fastmail.fm

TABLE OF CONTENTS

A Word from the Board

The State of Our Industry Update

By: Mihai Alexander Popovici, President

In November 2018, serving as First Vice President on the SEG Board I wrote a short article on the state of our industry looking at the evolution of the main service companies in our industry from 2012-2018 for the TLE President's Page that appeared in the December 2018 issue, you can find a copy here: https://library.seg.org/doi/10.1190/tle37120872.1 or here: http://www.alexanderbrad.com/2018/11/the-state-of-our-industry/

I decided to revisit the numbers in 2024, in the November 2018 article I had to estimate the revenues for 2018 as the data from the public companies was only available for the first two quarters, so I was curious to see how my estimate held against the real numbers. The approximation was pretty good for most of the companies, with a few others doing better, as you can see from comparing the old table with estimates with the new table with current numbers. Some companies restated their revenues post 2018, you will also find that comparing the two tables.

Mihai Alexander Popovici

My observation (and hope) that in 2018 "We are starting to pick ourselves up as an industry." was partially correct. The downturn started in 2014 and bottomed out in the middle of 2016. Then the industry revenues started to grow from the 2016 bottom through 2018 and 2019, then in 2020 Covid hit and the industry revenues took another dip. I was curious to learn if the second dip was lower or higher than the bottom in 2017. It turned out that it was about the same combined revenue value.

Year	Schlumberger	TGS	PGS	ION	Weatherford	Core Labs	Dawson	Halliburton	Baker Hughes	NOV	CGG
2012	42,010	932.24	1518	526.32	15,220	981	196	28,500		17,190	3414
2013	46,294	883.44	1502	549.17	15,263	1074	135	29,402	22,364	19,221	3768
2014	48,580	914.78	1454	509.56	14,911	1085	119	32,870	24,551	21,440	3097
2015	35,475	612.35	962	221.51	9433	798	235	23,633	15,742	14,757	2102
2016	27,810	455.99	764	172.81	5749	595	133	15,887	9841	7251	1197
2017	30,440	492	839	198	5699	660	157	20,620	17,259	7304	1321
2018 estimate	32,738	473	921	109	5767	695	158	24,181	22,043	8113	1191

Table 1: Service company revenues from 2012 to 2018 (in USD millions). Revenues for 2018 were estimated based on the first two quarters.

Looking at revenues of several publicly traded service companies (Table 2) over the past twelve years, it seems that on average the service industry took about a 60% hit from the highs in 2013 and 2014 to the low in 2016, as you can see in Figures 1 and 2. CGG was down from the peak of $3.768 billion in 2013 to $1.197 billion in 2016, a 68% drop. PGS was down from a $1.518 billion peak in 2012 to $764 million in 2016, a 50% drop. ION went from $549.17 million in 2013 to $172.81 million in 2016, a 69% drop. TGS went from $914.78 million in 2014 to $455.99 million in 2016, a 45% drop. Schlumberger went from $48.87 billion in 2014 to $28.01 billion in 2016, a 43% drop. Missing from the 2023 numbers is the ION revenue, which went bankrupt in 2022.

What can we learn from the numbers? It seems Baker Hughes and TGS did the best compared to their peers, their revenue recovered to 89.8% and 81.2% from their

Continued on page 3

TABLE OF CONTENTS

Year	SLB	TGS	PGS	ION	Weatherford	Core Labs	Dawson	Halliburton	Baker Hughes	National Oilwell Varco	CGG/Viridien
2012	42010	932.24	1518	526.32	15220	981	196	28500		17190	3,414
2013	46294	883.44	1502	549.17	15263	1074	135	29402	22364	19221	3,768
2014	48580	914.78	1454	509.56	14911	1085	119	32870	24551	21440	3,097
2015	35475	612.35	962	221.51	9433	798	235	23633	15742	14757	2,102
2016	27810	456	764	172.81	5749	590	138	15887	9841	7251	965
2017	30440	492	839	198	5699	648	157	20620	17259	7304	1,036
2018	32815	614	874	180	5744	701	154	23995	22877	8453	1,195
2019	32917	586	931	175	5215	668	146	22408	23838	8479	1,357
2020	23601	360	473	123	3685	487	86	14445	20705	6090	887
2021	22929	519	635	122	3645	470	25	15295	20502	5524	1063
2022	28091	717	825	0	4331	490	37	20297	21156	7237	927
2023	33135	794	867.463	0	5135	510	78	23018	22040	8583	1,076

Table 2: Service companies revenues from 2012 to 2023 (in USD millions). In yellow the peak revenue number for each company.

peak in 2013 and 2012 respectively. Then there is a second group of companies, Halliburton, SLB, PGS, Core Labs that recovered to 50-60% from the peak, and a third group that did not do that well, CGG, Weatherford, NOV.

And lastly Dawson and ION, at the bottom of the performance ranking table. Dawson was acquired by the Wilks Brothers, and ION went bankrupt in 2022. CGG (now Viridien) seems to be in trouble if you look at Figure 3, they have the lowest recovery-from-the-peak numbers.

How about the future? I was optimistic in 2018, I thought the industry was on a path to recovery, then the Covid lockdowns hit and the industry went downhill. Again. Barring some catastrophic event that I cannot predict, I think the industry will do well the next few years. Will it get back to the peak of 2014? I don't know. I hope so, but we lost a lot of good people. Maybe some will come out of retirement and maybe we'll get more students interested in the field as the job demand grows.

When I became President Elect of the Geophysical Society of Houston (GSH) I did the same analysis of the GSH revenues over the last 10 years. It turns out there is a very high correlation between society's revenues and the industry revenues. The society had peak revenues in 2014, then a big drop in the downturn 2014-2017, then a small recovery, then a second drop in the Covid pandemic, and now it is going up like the rest of the industry. I am optimistic about the future, I think better times are ahead of us as an industry and for GSH as well.

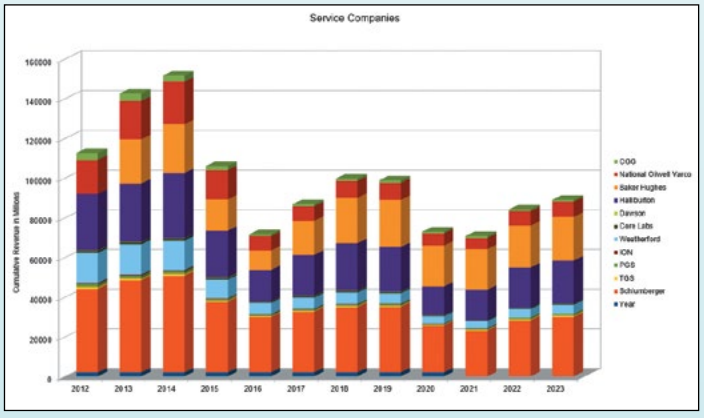

Figure 1: Total revenues from 2012 to 2023 for several service companies. 2023 revenues were estimated based on summing the last four quarters, which likely is a lower number than the final one.

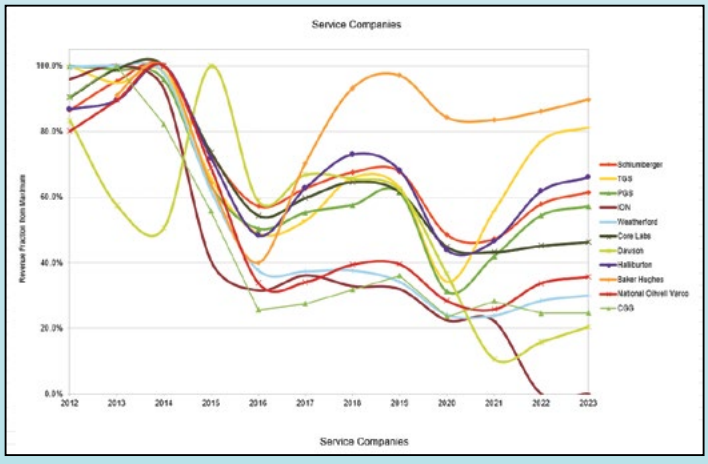

Figure 3: Normalized service companies revenues from 2012 to 2023.

Figure 4: GSH Total Revenues over the last 15 years.

TABLE OF CONTENTS

From the Other Side

By: Lee Lawyer, October 16th, 2024

Here I go again. I have written "From the Other Side" every month for about 20 years. That is a lot of columns but I enjoyed every one of them. I hope you did also. The GSH Journal is restarting the original Journal on a quarterly basis. If the GSH runs out of money, or you stop reading it, or both, the quarterly journal is subject to cancellation.

The GSH Journal has had some rough going over the last couple of decades. Back then, the GSH published the Journal in black and white. In a Board meeting, Mike Graul (then current President) suggested we jazz up the Journal with color and items of interest. That started an amazing five year run of exceptional Journals with Items like Tutorial Nuggets, A Conversation with…., Doodlebugger Diary, and several other items such as SIG reports, GSH Outreach, a technical paper and more mundane items like a President's Page and a report from a SEG Student Section at the University of Houston. All of this (Ten Journals per year) was printed and mailed to the subscribers. Later, we decided to move to "on line" to save money. We saved money and then we moved again to a modern style, which reduced the readership and the advertisers and me (gulp). If you are interested, copies of previous Journals are available to read at the GSH office and Library.

I used to have my picture at the heading of each column. One time the SEG stopped printing pictures of authors. I fought the Editor but was losing. I put a Neandertal in place of my picture. The Editor didn't catch it, as I recall. Oh well, I have decided to prove that I am old and need consideration. See the current picture which shows me on the back of a dinosaur about 60 million years ago….(Kidding, of course. I am not that old.).

I usually pick a subject and see if I can generate any interest with the readers. Consider an old subject that is still brewing, i.e., man-made climate change. Recall Al Gore's item entitled, 'An inconvenient fact" or something like that. The technical paper on that subject was written by a geologist from England (or Scotland). He stated that CO_2 was a greenhouse gas whose excess causes global warming. Not long ago, I conducted a survey at the GSH office during a meeting of the Living Legends. There were six or seven of us. I asked each one whether he/she believed that 'man' was causing global warming. Each voted that man was NOT responsible. Egad..

I attended the Annual SEG/AAPG meeting in Houston in late August. It was named IMAGE, which means walking from one end of the Convention Hall to the other. Wow. My first event was at the SEG Council. I was a "stand-in" if one of our three delegates failed to show. All three arrived. A few years ago, the GSH had six delegates. The number of Delegates is determined by the number of GSH/SEG members. The GSH has about 800(?) members today. At one time we had over 2,000 members (Where are you people?).

At IMAGE, I also listened to an event discussing geothermal energy, which means converting natural heat to usable energy. This is a very interesting subject. 'Geothermal Rising' is a 501-c3/501-c4 organization that quarterly produces a magazine entitled Geothermal Rising Bulletin. I picked up a 'Winter 2024, Volume 50, Issue 3'. They seem to have been around for quite a while. It discussed a project to evaluate the possibility of using 'dry heat', i.e., no water. I assume that means igneous rock with no permeability. In that case they must drill a hole, pump water down and recover it after it is heated by the 'dry heat'. That means they would need two holes to the objective. You know, one down and one up. I guess, they could put two liners (?) in one hole. Is it clear that I am not up to date on geothermal energy?…. but interested.

For questions, comments, suggestions, or what have you, contact me at **llawyer@prodigy.net**.

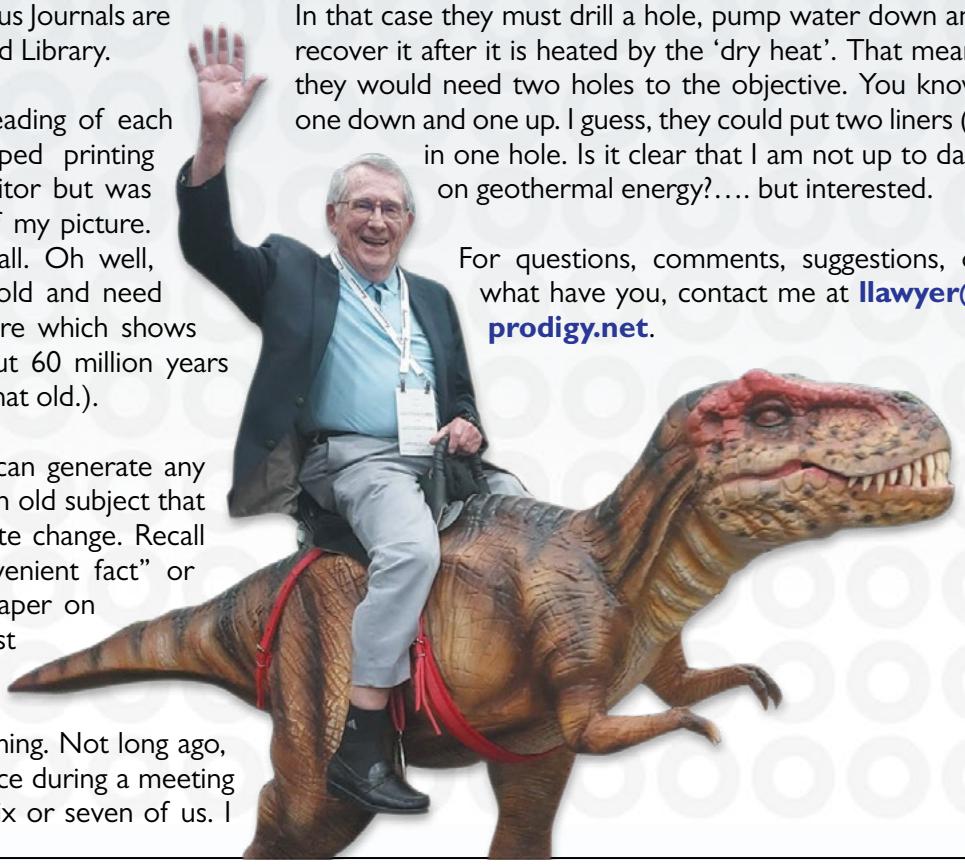

TABLE OF CONTENTS

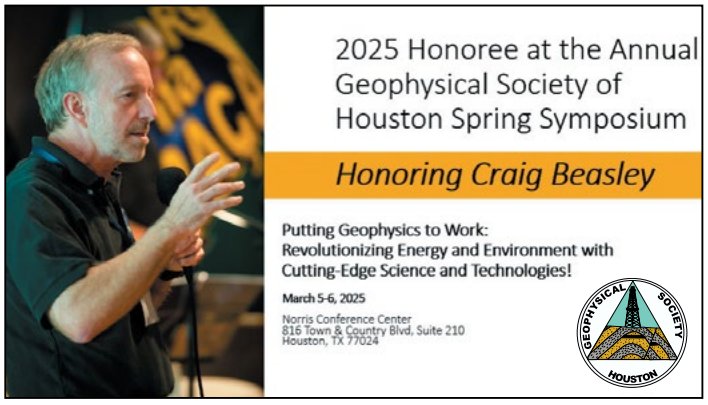

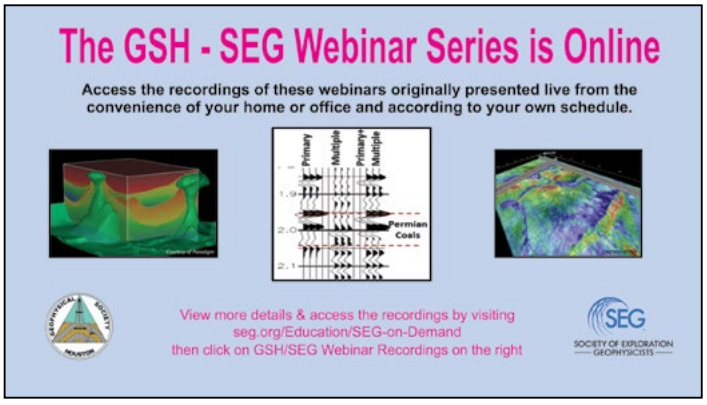

GSH Gets Down to Business a business-oriented online series

The traditional technical marketing meeting, whether it is a proprietary client in-house event or a booth presentation at a convention, is evolving. The GSH has an online commercial presentation series where companies are able to deliver information on their latest products and services to GSH members and friends! Key features are:

- A vendor offers their commercial presentation as an online event through GSH.
- The event is announced, promoted and managed by GSH; attendance is free.
- As in a booth presentation, both potential customers and competitors may be attending.
- After the presentation, there will be an interactive Q&A session.
- This is an excellent opportunity to present your product or service to a broad group of GSH members and associates.

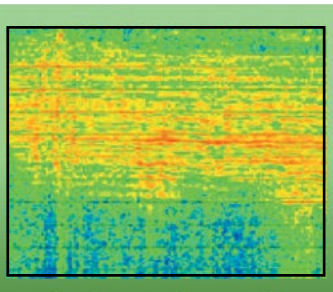

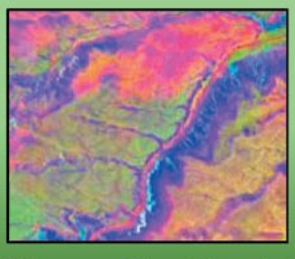

Interested vendors please contact the GSH at 281.741.1624 or office@gshtx.org

GSH Museum News

By: Bill Gafford (cypbill@gmail.com)

As we prepare items in our GSH Museum Collection for display, we try to discover some history of the items to indicate how they were used, their manufacturer, and their vintage.

One of the more interesting items is a borehole gravity meter, or BHGM, which is on display, along with the Iverson Gravity Collection, at Bell Geospace offices in North Houston. While this collection is part of the SEG collection, the GSH is the local custodian of the items. This meter was the first gravity meter deployed in a wellbore. A picture of this instrument and the associated control unit is included with this article. The following history and information is from Ted Lautzenhiser and Bill Jones who were involved in the original development and operation of the BHGM at Tidelands, Gravilog, and Amoco.

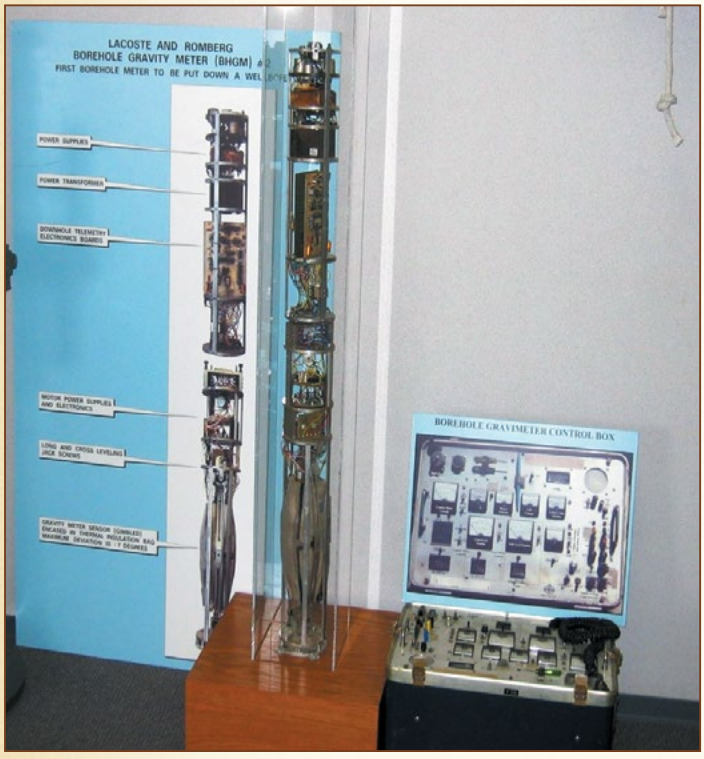

"The meter on display is LaCoste & Romberg BHGM #2, which was originally funded by a consortium of seven oil companies, including Amoco, who was the operator for the group. For testing and subsequent usage it was given to Tidelands Geophysical in Houston to operate around 1970. The electronics for BHGM #2 were designed by a professor at Rice University and subsequently upgraded to work better in a borehole. I think the first successful production for Amoco resulting from a BHGM survey was in the Hastings field, in SE Houston. Around 1972 Gravilog was split off from Tidelands to continue supplying BHGM services. Tidelands and then Gravilog had received several of the vibrating string BHGMs from Humble, who had used them successfully in Libya, but which were not accurate enough for the smaller production fields in the USA. We could not utilize them commercially because of their accuracy limitations, but we tried. LaCoste& Romberg BHGM #3 was bought by Gravilog with 120 degree centigrade operating temperature as opposed to No. 2's 105 degrees. In 1975 Amoco bought the BHGM's. Several more meters of advanced operating ranges were instrumented by Amoco as LaCoste & Romberg continued to increase the operating temperature and decrease the tool diameter, from the 5 1/2 inches of No. 2 & 3 to 4 1/4 inches for the later meters. The meters had good commercial success in the Michigan Reef plays, Gulf Coast and the over-thrust play in Colorado and Wyoming."

"Amoco had more early success with borehole gravity surveys than any other company. Their first big success was in Michigan where they were developing small reefs. As often happens, the success was to some extent luck. The porosity in the reefs was vugular and finding zones of porosity was hit and miss. Amoco had drilled several reefs which had good oil and gas shows but according to the gamma logs, zero or chose to it, porosity. We had a crew in Traverse City on another project when Amoco TD'd another such well. I don't know who decided to do it but someone in Amoco decided to run a borehole gravity survey in the well. The idea was to compare the densities from a conventional density log with those from the borehole gravity log. If there was a discrepancy it might indicate a zone of porosity close enough to the well bore to be reached by acidizing the zone. There were three such zones in the well and the technique worked with spectacular success."

"Gravilog/Amoco retrofitted BHGM #2 and #3 with new electronic packages. Subsequent Amoco meters used Amoco developed electronics during testing at LaCoste and Romberg in Austin and in field usage. Amoco tested all the meters in an Amoco well AK 199 north of Midland-Odessa. Tidelands/Gravilog also tested the meters in an Exxon test well south of Houston also in the Hastings field. Edcon Inc. in Denver was getting into the BHGM business after the Gravilog/Amoco successes with the original meters and got several of the Amoco meters when Amoco decided to get out of the survey business in 1975."

I would welcome additional historical information on this item or others in our Museum collection.

TABLE OF CONTENTS

Assessing the CO_2 Sequestration Potential of the Paleogene Wilcox Group, Onshore Texas, USA

Carlos A. Uroza, Mariana I. Olariu, Maria Madariaga, Shuvajit Bhattacharya, and Susan Hovorka
Bureau of Economic Geology, University of Texas at Austin

Abstract

We present a comprehensive subsurface assessment to evaluate the Wilcox Group CO_2 sequestration potential in a 590 km transect, from SW Texas to the limit with Louisiana. Subsurface evaluation included: 1- well-log correlation to identify the Wilcox stratigraphic units and their continuity, 2- 2D seismic interpretation to assist the identification of major structural elements in the area of interest, 3- structural and sand mapping to identify structural lows with enough sand presence for CO_2 storage, 4- sedimentological analysis to understand the aerial distribution of depositional facies in support of GDE mapping, 5- salinity analysis of Upper Wilcox/Carrizo Fm. aquifer to identify and map the base of the USDW (define the no-go areas for CO_2 sequestration), 6- petrophysical evaluation to estimate the reservoir properties in the Wilcox Group and evaluate the controls on reservoir quality, and 7- CO_2 storage capacity estimations, using EASiTool software, in areas with low structural complexity and low well penetrations.

The research demonstrated the feasibility of the Wilcox Group for CO_2 storage, especially in the central and eastern areas of the studied transect where the USDW is shallow enough to avoid contact with the Wilcox storage window. The study provided an opportunity to review the Wilcox depositional system within the studied transect to allow for the identification of main sand depocenters for storage site consideration. It represents a first pass to investigate the CO_2 sequestration potential of the Wilcox. A trend capacity estimation is not provided due to regions with a large number of legacy wells that may need to be avoided by project developers to reduce the chance of leakage.

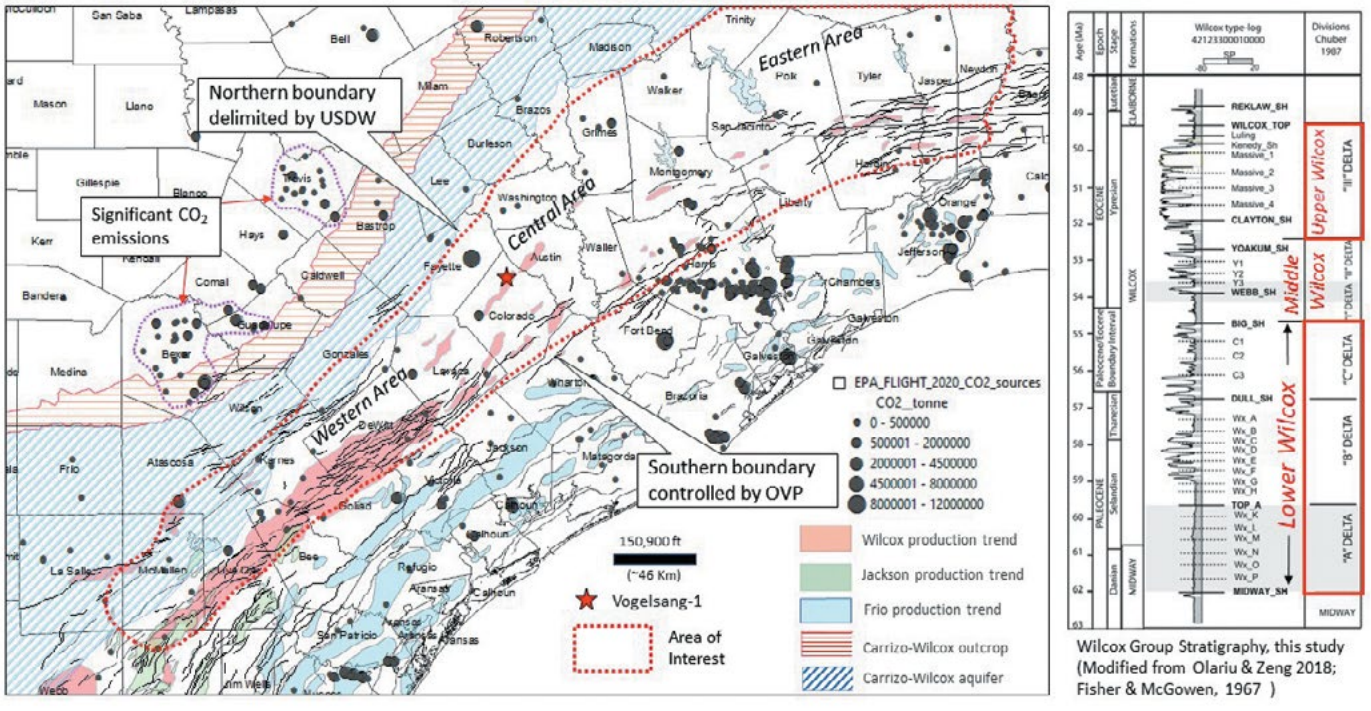

Wilcox Group Stratigraphy, this study (Modified from Olariu & Zeng 2018; Fisher & McGowen, 1967)

Figure 1. Area of interest Wilcox study (outlined in dashed red polygon). Northern boundary delimited by USDW and southern boundary delimited by overpressure. Also shown, stratigraphic column Wilcox Group with subdivisions used in this study.

Continued on page 9

TABLE OF CONTENTS

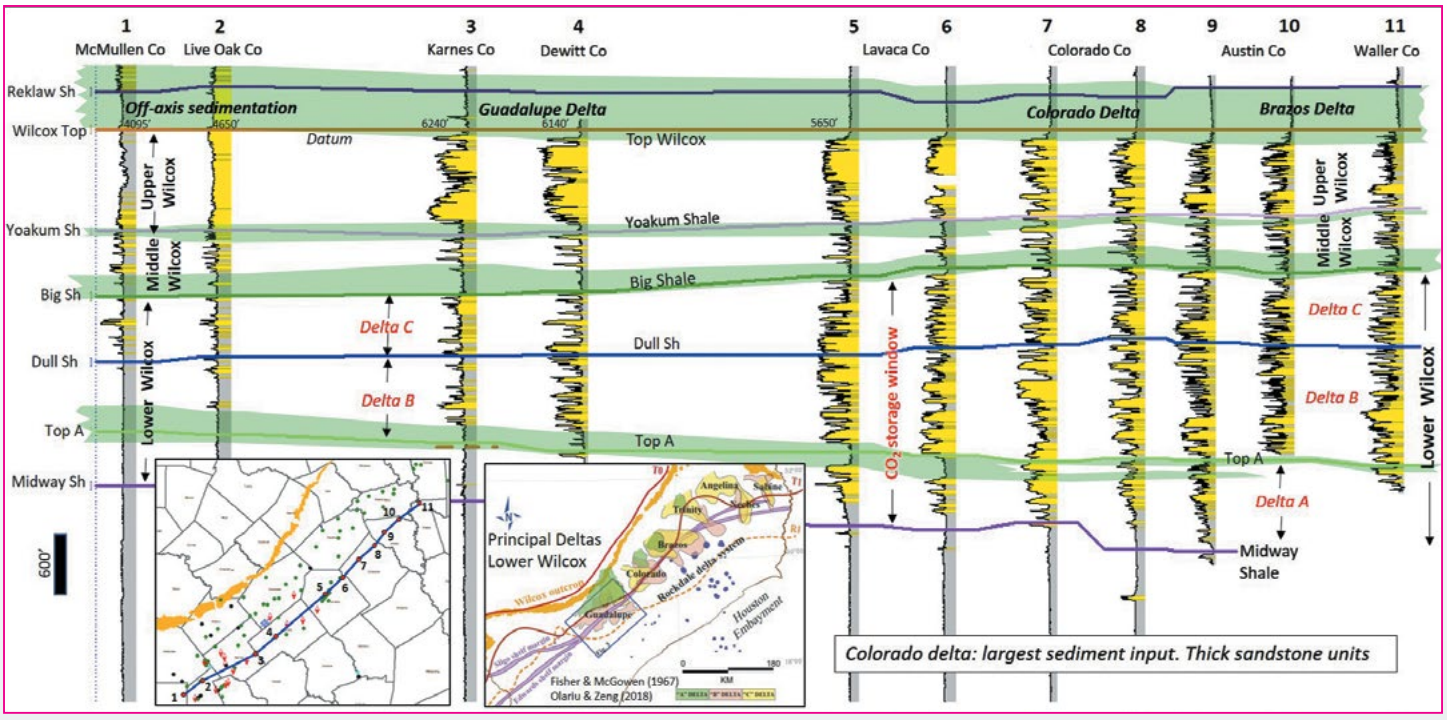

Figure 2. Stratigraphy of the Wilcox Group, western and central areas. Lateral variability in sand presence influenced by the corresponding sediment delivery system, i.e., paleo Colorado river-delta system in Colorado county.

Introduction

The Wilcox Group is well-known for its substantial hydrocarbon accumulations in the Gulf of Mexico basin. Onshore, it hosts important underground sources of drinking water (USDW) with salinity below 10,000 ppm that require protection under the USA Environmental Protection Agency rules (US EPA, 2013). Many studies were done for the assessment of such hydrocarbon and water resources (Fisher & McGowen, 1967; Loucks et al., 1984; Hamlin & de la Rocha, 2015). However, the Wilcox Group suitability for geologic CO_2 sequestration is little known. As for CO_2 sources, there are significant emitters around the study area (Figure 1).

The Wilcox Group onshore Texas is a sand-prone clastic system with thick sandstone units and good-to-moderate reservoir quality, which is important for CO_2 storage and injectivity. The Lower and Upper Wilcox represent the favorable stratigraphy and reservoir quality for CO_2 storage. Middle Wilcox contains mud-prone facies with limited storage potential. Lower Wilcox is capped and confined by the Big Shale, a thick and extensive interval of marine transgression. Upper Wilcox/Carrizo Formation is confined by the mud-prone Reklaw Formation. CO_2 storage window in the AOI is limited by the USDW depth to the north and depth of overpressure to the south. In the western area of the studied transect, a significant portion of the Upper Wilcox/Carrizo Fm. rests within the USDW, and cannot be considered for CO_2 sequestration. However, in the central and eastern areas the USDW is located above the Upper Wilcox/Carrizo Fm., providing a thicker section for CO_2 storage.

The western area (Figure 1) has been well documented by several authors (i.e., Olariu & Ambrose, 2016; Olariu & Zeng, 2018). However, the central and eastern areas are sparsely documented, so this study represents an opportunity to update the knowledge of the Wilcox Group in these areas. A master thesis recently conducted in the central area is part of this study (Madariaga, 2024).

Methods

- Extensive well-log correlation, using 100s of wells, along the 590 km transect (Figures 2 & 3). Correlation follows Olariu & Zeng 2018 stratigraphic subdivision (Figure 1). Well correlations were fundamental for structural and sand mapping, and to understand the aerial distribution of sandy reservoirs.

- 2D seismic interpretation, using the Gulf Coast ION dataset, to assist the identification of major structural elements in the AOI. Seismic coverage was limited since 2D lines are spaced tens of km apart.

Continued on page 10

TABLE OF CONTENTS

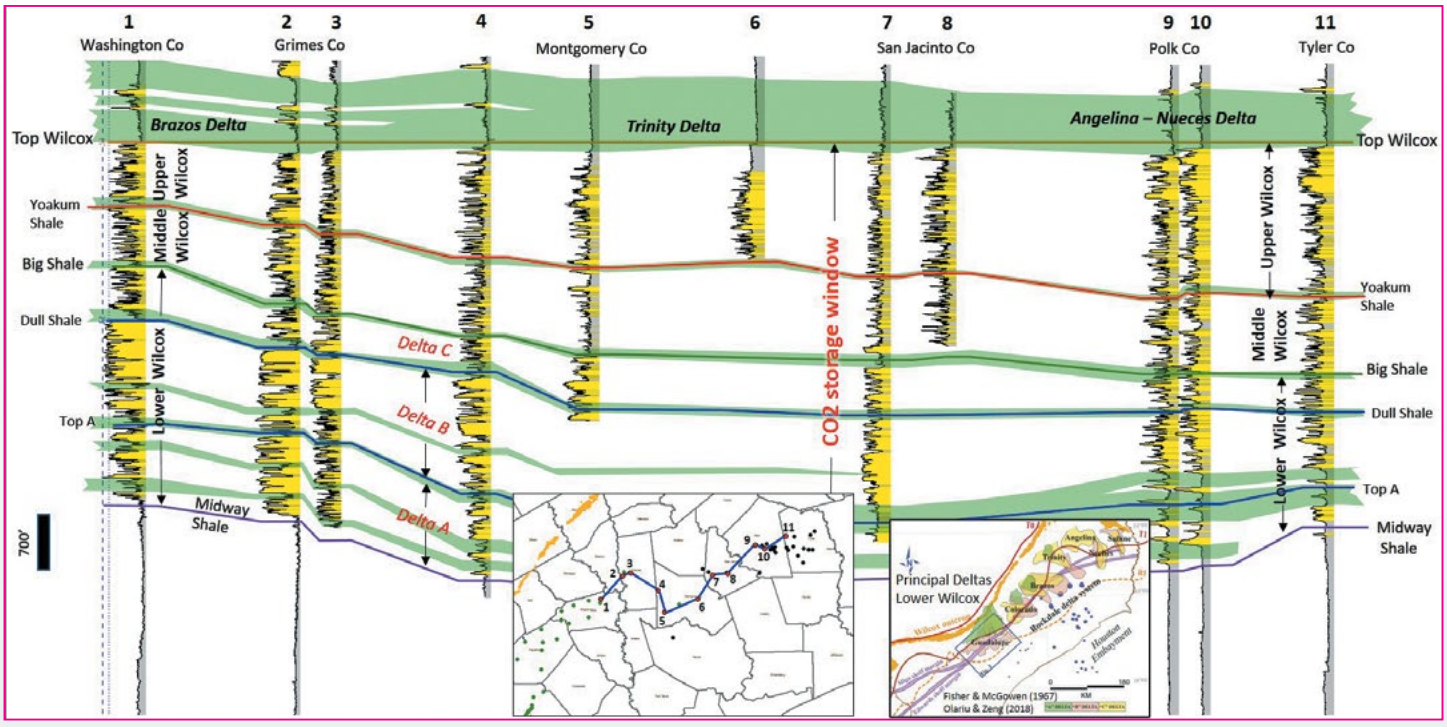

Figure 3. Stratigraphy of the Wilcox Group, central and eastern areas. Lateral variability in sand presence influenced by the corresponding sediment delivery system, i.e., paleo Brazos river-delta system in Washington county.

- Structural mapping, based on well logs, to identify structural lows in the AOI. The fault framework from Ewing (1991) was incorporated to the mapping, and in some cases the 2D seismic allowed validation of the location of main normal faults. Sand mapping helped to identify main sandy fairways and locate areas with enough sand presence for CO_2 storage (Figure 4 & 4-bis).

- Sedimentological analysis, using cores and well logs, to define depositional facies and understand their aerial distribution in support of GDE mapping. A few cores from western area and a long core from central area represent the basis for the facies analysis.

- Formation water salinity analysis of the Upper Wilcox/Carrizo Fm. to identify the USDW (TDS < 10,000 ppm). TDS (Total Dissolved Solids) calculations were completed for many wells, using empirical relationship between Ro (resistivity of a brine-saturated formation) and the formation water salinity. The base of the USDW was mapped to delineate the no-go areas for CO_2 sequestration.

- Petrophysical evaluation, with cores and well logs, to estimate reservoir properties in the Wilcox and to evaluate the controls on reservoir quality. Capillary pressure data was incorporated to the analysis, and grouped by depositional facies (Figure 5) to identify preferential facies for CO_2 flow and the ones that can prevent such flow.

- CO_2 storage capacity estimations in areas with low-density well penetration (Figure 6) using EASiTool, a non-commercial analytical software developed by Gulf Coast Carbon Center – Bureau of Economic

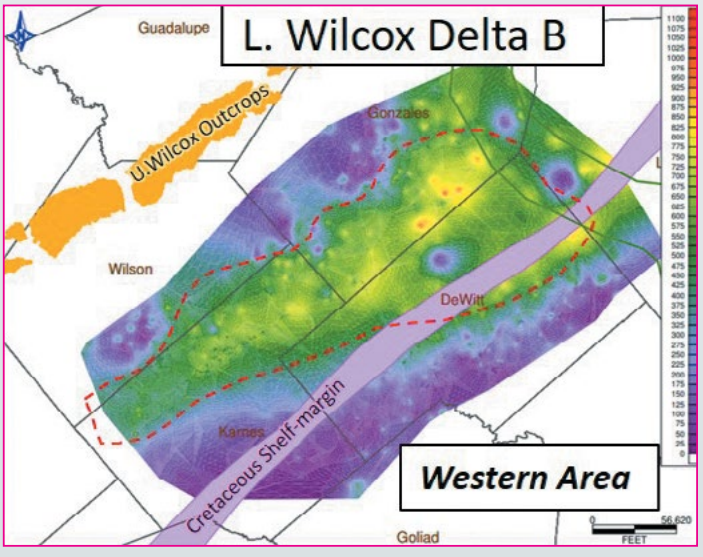

Figure 4. Sandstone maps and depositional trends for Delta B, Lower Wilcox, in western area.

Continued on page 11

TABLE OF CONTENTS

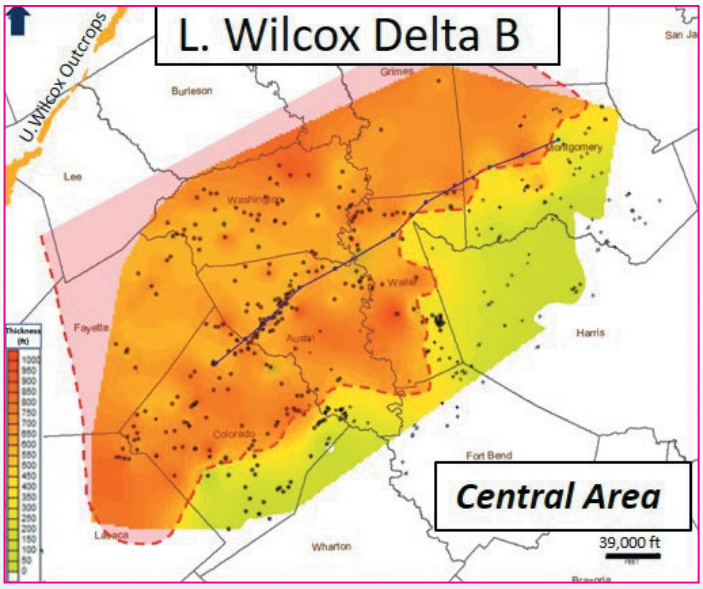

Figure 4-bis. Sandstone maps and depositional trends for Delta B, Lower Wilcox, in central area.

Geology, to model pressure buildup associated with CO_2 injection and brine extraction (Ganjdanesh & Hosseini, 2017, 2018). Initial reservoir pressures were considered as hydrostatic (saline aquifers) and maximum injection pressure ~ 85 % of fracture pressure.

Results

Well correlations and sand mapping along the studied transect show important variability in reservoir thicknesses, which it's attributed to the corresponding sediment delivery system. The westernmost area shows sediment bypass (Figure 2) due to its off-axis location. East of this area, we encounter the paleo Guadalupe delta, with moderate sand content in Lower Wilcox but sandier in Upper Wilcox (Figures 2 & 4). Though, the presence of a deep USDW in this area would limit the available stratigraphy for CO_2 storage. The central area of the studied transect contains the thickest sand development in the Wilcox Group, especially Lower Wilcox, as seen in well correlation and sand mapping (Figures 2 & 4-bis). Fisher & McGowen (1967) originally proposed an important Lower Wilcox constructional delta phase along the axes of the modern Colorado and Brazos rivers. The eastern area within the studied transect shows more interbedded sandstones and shales (Figure 3), which contrasts with the abundant blocky sandstone packages seen in the central area. In both central and eastern areas, the USDW is relatively shallow, so both Upper and Lower Wilcox are available for CO_2 storage.

Growth faulting played an important role in Lower Wilcox by creating space for accommodation, which

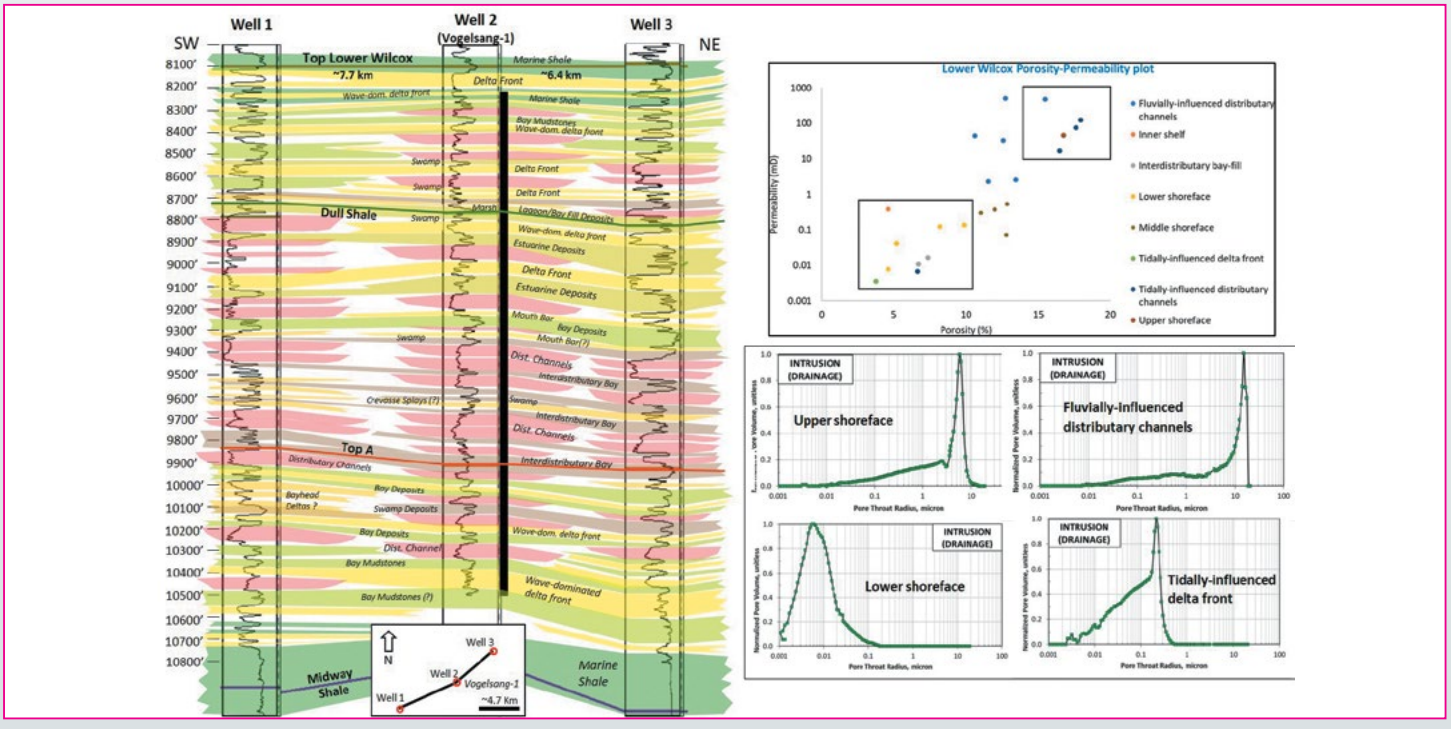

Figure 5. ***Left:*** *Depositional environments from Vogelsang-1 core, extrapolated to neighbor wells.* ***Right:*** *Controls on reservoir quality: Rock types defined by ϕ, k, and Pc*

Continued on page 12

TABLE OF CONTENTS

was filled with abundant deltaic sands, as it's the case for the paleo Colorado delta in the central area. Here, the Lower Wilcox reached thicknesses of more than 2500 feet (uncompacted). The evaluation of the Vogelsang-1 core from the central area (Figure 5) provided a good understanding of the Lower Wilcox depositional facies; however, lateral facies variability occurs along the studied transect. It's common to see blocky features in electrical logs from central area, which should be associated with stacked distributary channels.

Based on our available core data, reservoir quality within the Wilcox Group can be variable, with porosities and permeabilities ranging from 0.16 to 0.26 and 5 to 80 md, respectively, in the western area. The Vogelsang-1 core from the central area provided a good insight into the reservoir quality. In this area, porosity and permeability range from 0.12 to 0.2 and 1 to 120 md, respectively. Integration of capillary pressure analysis, grouped by depositional facies, show the fluvially-influenced distributary channels with pore throat radius exceeding 10 microns as the preferential depositional facies for CO_2 injection, while other depositional facies, such as lower shoreface may work as barriers to flow (Figure 5). Porosity decreases towards the south of the studied transect since burial and compaction increase.

For calculation of CO_2 storage capacity, we identified a number of areas with sufficient sand presence, not complex structurally, and with relatively low number of legacy wells to minimize risk of leakage. CO_2 storage capacity is more promising in the central and eastern areas of the transect, where the USDW is shallower than the Upper Wilcox top. Figure 6 shows an example of the storage capacity estimation for a 540 km^2 site in the central area. The storage capacity for this particular site is 289 Mt (Madariaga, 2024). By adding multiple sites along the studied transect we could reach gigaton-scale capacity in relatively good quality sandstones. Future studies should include possible pressure interference from multiple injection sites and how to derisk and optimize the storage capacity.

Conclusion

This Wilcox regional assessment has significance due to growing interest in CO_2 onshore storage. There are many emitters north of the studied transect (i.e., Austin and San Antonio areas) that would benefit from sandstone units providing good storage, containment, and injectivity. Pipeline cost needs to be considered in the economic analysis since potential storage sites are not closely located from CO_2 sources, with a few exceptions like Sam Seymour Power Plant, in Fayette county, which it's located 15 km from the proposed site in Figure 6 (Madariaga, 2024).

Based on well correlation and sand mapping of the deltaic Wilcox units, we conclude that there is significant CO_2 storage capacity along the studied transect, especially

Input Parameters

Parameter	Delta III	Delta C	Delta B
Depth (ft)	6190	7742	10272
Pressure (MPa)	20	25	33
Temperature (°C)	57	71	94
Thickness (m)	50	66	144
Porosity (%)	0.26	0.16	0.12
Permeability (mD)	80	30	5

Storage Capacity (Mt*)

Site A	Closed Boundary (Mt)	Open Boundary (Mt)
Delta III	128	164
Delta C	46	137
Delta B	115	121
Total	**289**	**422**

Mt* = Megatons (Million Metric tons)

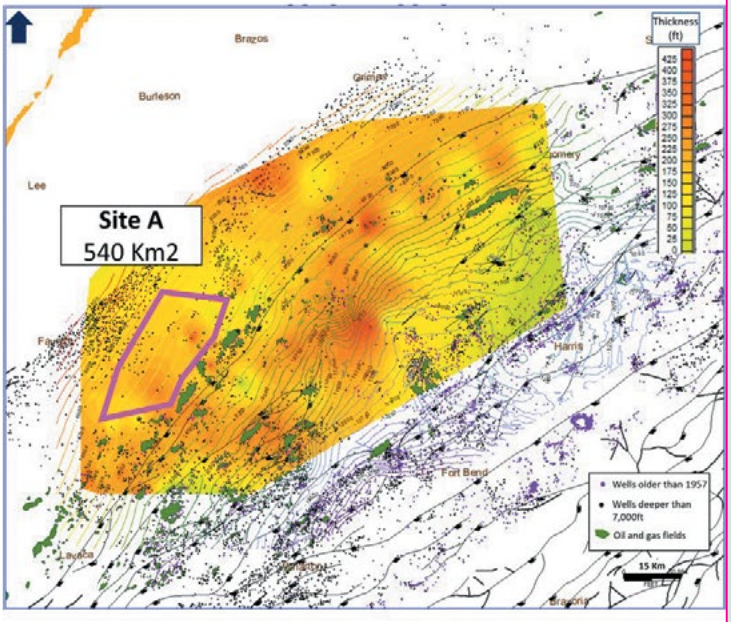

Figure 6. Example of storage capacity calculation from central area, using EASiTool (courtesy of Maria Madariaga, MSc thesis 2024)

Continued on page 14

TABLE OF CONTENTS

The GSH - SEG Webinar Series is Online

Access the recordings of these webinars originally presented live from the convenience of your home or office and according to your own schedule.

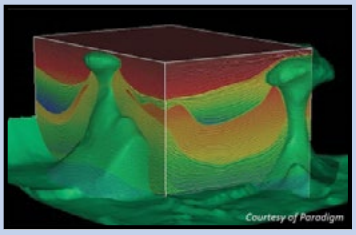

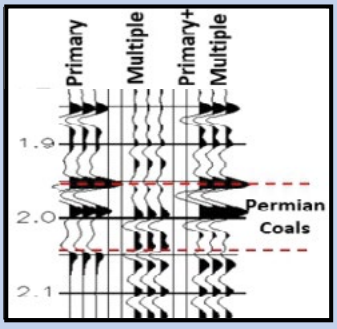

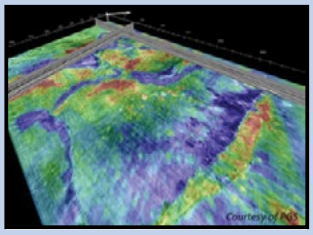

Title	Presenter
– Seismic Modeling, Migration, and Inversion	Bee Bednar
– Beyond AVO to Quantitative Inversion Interpretation QII	Bill Goodway
– Affordable S-Wave Reflection Seismology	Bob Hardage
– Simplifying and Lowering the Cost of S-Wave Reflection Seismology	Bob Hardage
– Carbonate Essentials	Chris Liner
– Basic Seismic Interpretation	Don Herron & Bob Wegner
– Basics and UPDATES on Anisotropy: Azimuthal P-P for better Imaging, Fractures & Stress Analysis Acquisition, Processing & Interpretation	Dr. Heloise Lynn
– Geophysical Signal Processing 101	Enders A. Robinson & Sven Treitel
– Seismic Amplitude 20/20: An Update and Forecast	Fred Hilterman & Mike Graul
– Extracting Geology from Seismic Data	Fred Schroeder
– Applied Azimuthal Anisotropy-Azimuthal 3D P-P Seismic: WHY Bother?	Dr. Heloise Lynn
– Understanding Seismic Anisotropy in Exploration and Exploitation	Leon Thomsen
– An Introduction to Borehole Acoustics	Matthew Blyth
– Topics in Land Seismic Data Acquisition, Processing, & Inversion	Oz Yilmaz
– Everything You Always Wanted to Know About Microseismic Monitoring	Peter Duncan
– Full-Wave Seismic Exploration: Acquisition, Analysis, & Applications	Rob Stewart
– Introduction to Applied Depth Imaging	Ruben D. Martinez
– The Interpreter's Guide to Depth Imaging	Scott MacKay
– Machine Learning Essentials for Seismic Interpretation	Tom Smith
– Modern Seismic Reservoir Characterization	Leon Thomsen
– Borehole geophysics: Using rock properties, well logs, & all kinds of seismic methods	Rob Stewart

View more details & access the recordings by visiting
seg.org/Education/SEG-on-Demand
then click on GSH/SEG Webinar Recordings on the right

SOCIETY OF EXPLORATION GEOPHYSICISTS

in central and eastern areas where a shallow USDW allows for more pore volume to be filled with CO_2. The environments of deposition (EOD) are variable along the transect, where delta front and fluvial distributary channels make the most attractive sandy units for storage. Delta front sandstones would exhibit better lateral continuity, allowing better dissipation of the injected CO_2. High permeable channels, mainly oriented N-S or NW-SE, can be preferential fairways for the injected CO_2. Such variability in depositional facies needs to be properly modelled to better predict the CO_2 movement in the subsurface.

Reservoir quality is also variable, and needs to be analyzed site by site. It is mostly controlled by the depositional facies, burial and compaction. Diagenesis seems to play a lower role in controlling the Wilcox reservoir quality.

Acknowledgments

This study was funded by the US Department of Energy under DOE Award Number DE-FE0031830, Southeast Regional CO_2 Utilization and Storage Acceleration Partnership (SECARB-USA).

References

i. Ewing, T. E., 1991, The tectonic framework of Texas: Bureau of Economic Geology, Austin, Texas.

ii. Fisher, W. L., and McGowen, J. H., 1967, Depositional systems in the Wilcox Group of Texas and their relationship to occurrence of oil and gas: Transactions – Gulf Coast Association of Geological Societies, XVII, 105-125.

iii. Ganjdanesh, R., andHosseini, S. A., 2017, Geologic carbon storage capacity estimation using enhanced analytical simulation tool (EASiTool): Energy Procedia, 114, 4690–4696.

iv. Ganjdanesh, R., and Hosseini, S. A., 2018, Development of an analytical simulation tool for storage capacity estimation of saline aquifers: International Journal of Greenhouse Gas Control, 74, 142–154.

v. Hamlin, H. S., and de la Rocha, L., 2015, Using electric logs to estimate groundwater salinity and map brackish groundwater resources in the Carrizo-Wilcox aquifer in south Texas: GCAGS Journal, 4, 109–131.

vi. Loucks, R.F., Dodge, M.M., and Galloway, W.E., 1984, Regional controls on diagenesis and reservoir quality in Lower Tertiary sandstones along the Texas Gulf Coast: AAPG Memoir, 37, 15-45.

vii. Madariaga, M., 2024, Assessment of CO_2 storage potential of the Wilcox Group in an onshore region of Texas: MSc thesis, The University of Texas at Austin.

viii. Olariu, M. I., and Ambrose, W. A., 2016, Process regime variability across growth faults in the Paleogene Lower Wilcox Guadalupe Delta, South Texas Gulf Coast: Sedimentary Geology, 341, 27–49.

ix. Olariu, M. I., and Zeng, H., 2018, Prograding muddy shelves in the Paleogene Wilcox deltas, south Texas Gulf Coast: Marine and Petroleum Geology, 91, 71–88.

x. US EPA, 2013, Underground Injection Control (UIC) Program Class VI Well Site Characterization Guidance, https://www.epa.gov/sites/default/files/2015-07/documents/epa816r13004.pdf

TABLE OF CONTENTS

AI-Powered Lithofacies Prediction and Fault Detection in Complex Thin Gas Reservoirs Offshore Eastern India

Fabian Rada, Alvaro Chaveste, Rocky Roden, Tom Smith, and Michael Dunn
Geophysical Insights, Houston, Texas

Abstract

Accurately predicting lithofacies and detecting faults in thin, compartmentalized gas reservoirs is challenging due to complex stratigraphy and limited data resolution. This study addresses these challenges in an Offshore area in Eastern India, where one well intersects thin Pleistocene gas sands. Traditional lithofacies prediction methods, such as seismic inversion, are often constrained by the quality and extent of data. We applied K-means clustering to well log data and used Self-Organizing Maps (SOM) on multi-attribute seismic volumes to develop a high-resolution lithofacies model. This process produced a 95% match between lithofacies from logs and lithofacies from seismic. Convolutional Neural Networks (CNN) further refined fault detection, enhancing the structural understanding of reservoir compartments. Integrating these AI-driven methods resulted in a unified model of lithofacies and faults, significantly improving reservoir characterization. This approach offers an efficient alternative to conventional methods, aiding connectivity assessment and informing exploration strategies in complex geological settings.

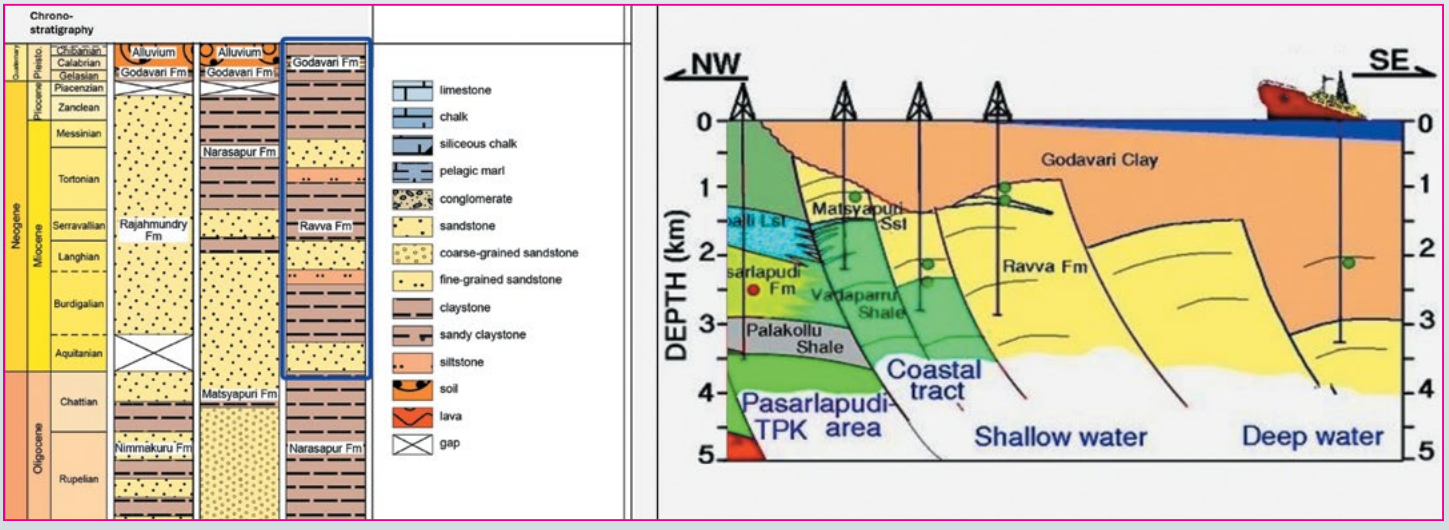

Figure 1. ***Left:*** *Cenozoic stratigraphy of the basin (modified from Indian Plate Lexicon of Stratigraphic Units, 2024).* ***Right:*** *Geological section (modified from Harikrishna et al., 2023).*

Introduction

Lithofacies prediction and fault detection in thin, highly compartmentalized gas reservoirs pose significant technical and geological challenges. Complex stratigraphic and structural features hinder hydrocarbon flow and complicate connectivity assessment across reservoir blocks. In this study area, there is only one well intersecting a few thin, gas-bearing Pleistocene sandstones. The limited quantity and variable quality of well data often constrain robust characterization, while the seismic data's insufficient vertical resolution further challenges the detection of thin reservoirs.

Traditional lithofacies prediction relies on rock physics, expected geological trends, and techniques like amplitude versus offset (AVO) analysis and seismic inversion (Avseth et al., 2005; Mavko and Mukerji, 2009; Dvorkin

Continued on page 18

TABLE OF CONTENTS

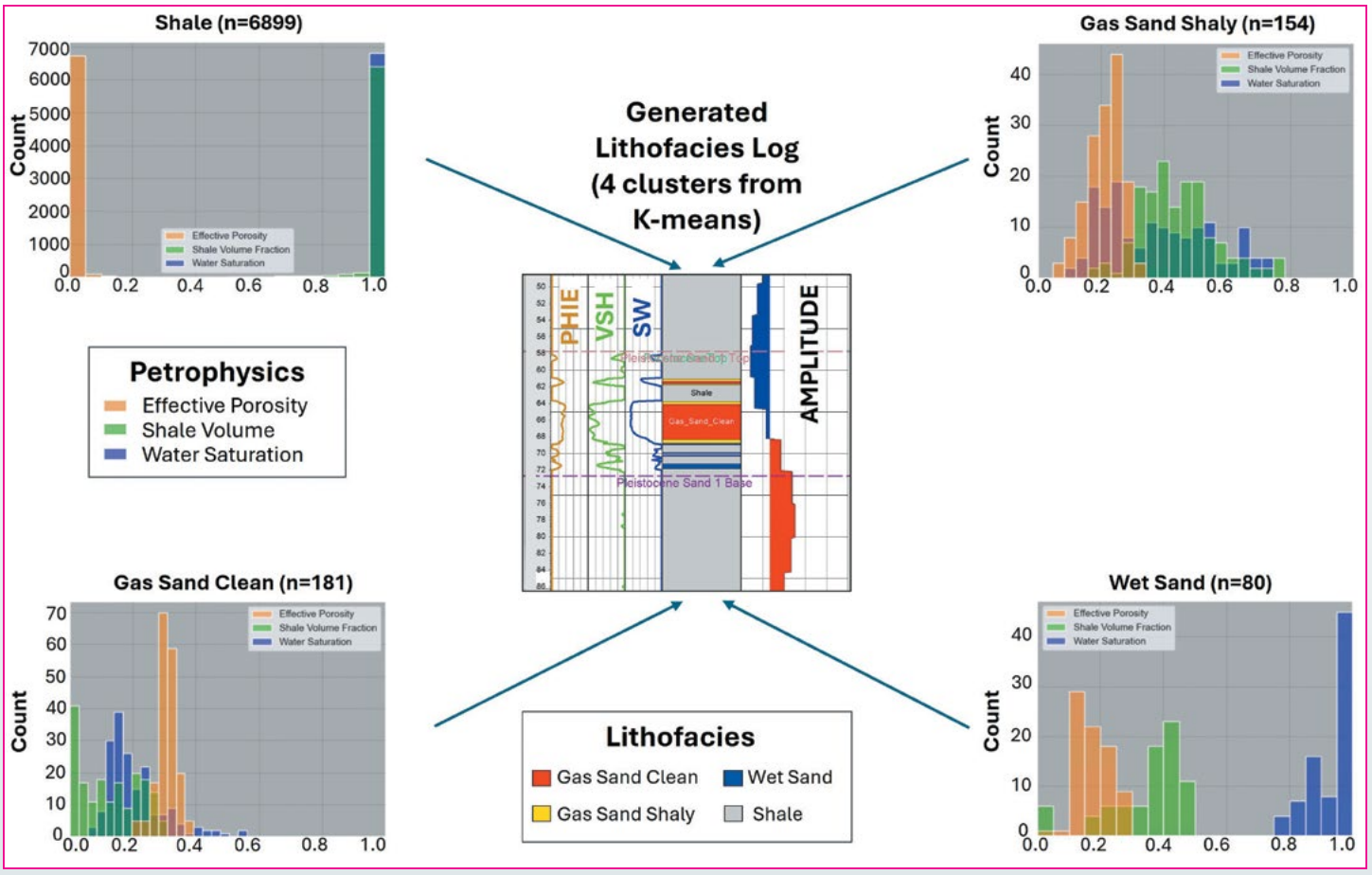

Figure 2. Lithofacies log using three petrphysical curves: PHIE, VSH and SW, clustered by K-means in four lithofacies: Shale, Gas Sand Clean, Gas Sand Shaly and Wet Sand.

and Nur, 1996). These approaches, though powerful, require extensive expertise, high-quality data, and are often costly, especially in heterogeneous, low-resolution areas (Russell and Hampson, 1991; Veeken and Silva, 2004). In this context, artificial intelligence (AI) offers a promising alternative. Neural networks and classification algorithms, like SOM, are powerful nonlinear cluster analysis and pattern recognition techniques that help geoscientists identify patterns that can be related to lithofacies (Chaveste et al., 2023).

In this study, AI predicts lithofacies volumes by combining K-means clustering of well log data with multi-attribute seismic classification volumes sampled at a 4-millisecond interval. This approach can match or exceed traditional inversion methods in accuracy, with less human intervention and greater tolerance for incomplete data. Additionally, convolutional neural networks (CNN) were employed to generate fault classification and probability volumes (Wu et al., 2019), which, alongside lithofacies volumes, help unravel the area's complex stratigraphic and structural framework, essential for constructing static and dynamic reservoir models.

Geologic Setting

This study is in a peri-cratonic passive margin basin off the east coast of India (Gupta, 2006). The basin has a layered tectono-sedimentary history shaped by rifting and sedimentation, with two major tectonic phases. This study focuses on the Rajahmundri Sandstone and Ravva Formation. The Ravva is glauconitic and calcareous, while the Rajahmundri is medium-grained and lateritized. Pleistocene-Miocene sedimentation created a complex structure with growth faults, intraslope lobes, and bypass channels (Figure 1).

Methodology

Machine Learning (K-means) for Lithofacies Log Generation

K-means clustering is highly valued in petroleum engineering for classifying well log data due to its efficiency with large datasets common in reservoir analysis. Its straightforward

Continued on page 19

TABLE OF CONTENTS

iterative approach enables rapid processing of data across various reservoir scales (Han et al., 2011). When applied to high-dimensional well log data, such as porosity, resistivity, and permeability, K-means effectively uncovers patterns within these various data types to identify lithofacies and assess reservoir quality (Jain et al., 2010).

A significant advantage of K-means is its interpretability; each cluster centroid represents the average properties of a lithofacies, aiding geoscientists in evaluating reservoir characteristics. Compared to more complex algorithms like SVMs or Neural Networks, K-means produces clusters that are easier to interpret, which is valuable for initial exploratory analysis when labeled data may be unavailable or costly (Chen et al., 2018). Additionally, K-means is highly scalable, processing data across numerous wells effectively. By selecting an optimal number of clusters (K), the approach can adapt to specific geological needs for a more comprehensive reservoir characterization. In this study, clustering used Effective Porosity, Volume of Shale, and Water Saturation as input properties. Initially, eight clusters were established, and histograms of each petrophysical curve response helped define four lithofacies: Gas Sand Clean, Gas Sand Shaly, Shale, and Wet Sand.

Machine Learning (Self-Organizing Maps) for Multi-Attribute Volume Generation

The seismic data used in this study originates from a Pre-Stack Time Migration amplitude volume, with a 4-millisecond sample interval and 12.5 meters squared bin size. This amplitude volume served as the base for generating eleven instantaneous seismic attributes: Phase Acceleration, Attenuation, Bandwidth, Envelope, Envelope Slope, Envelope Second Derivative, Hilbert, Instantaneous Frequency, Relative Acoustic Impedance, Sweetness, and Thin Bed. These attributes were classified simultaneously through the Self-Organizing Maps (SOM) neural network (Kohonen, 1982). Smith and Treitel (2015) stated that Self-organizing maps at single sampling interval are a practical way to identify natural clusters in multi-attribute seismic data. Here, the SOM volume was transformed into a log along the well path, allowing direct statistical comparison with the K-means lithofacies log, allowing the geoscientists to link both types of data through the Lithofacies Prediction tool in Paradise®.

Fault Detection Using Deep Learning

The Convolutional Neural Network (CNN) was trained using thousands of synthetic volumes with variations in

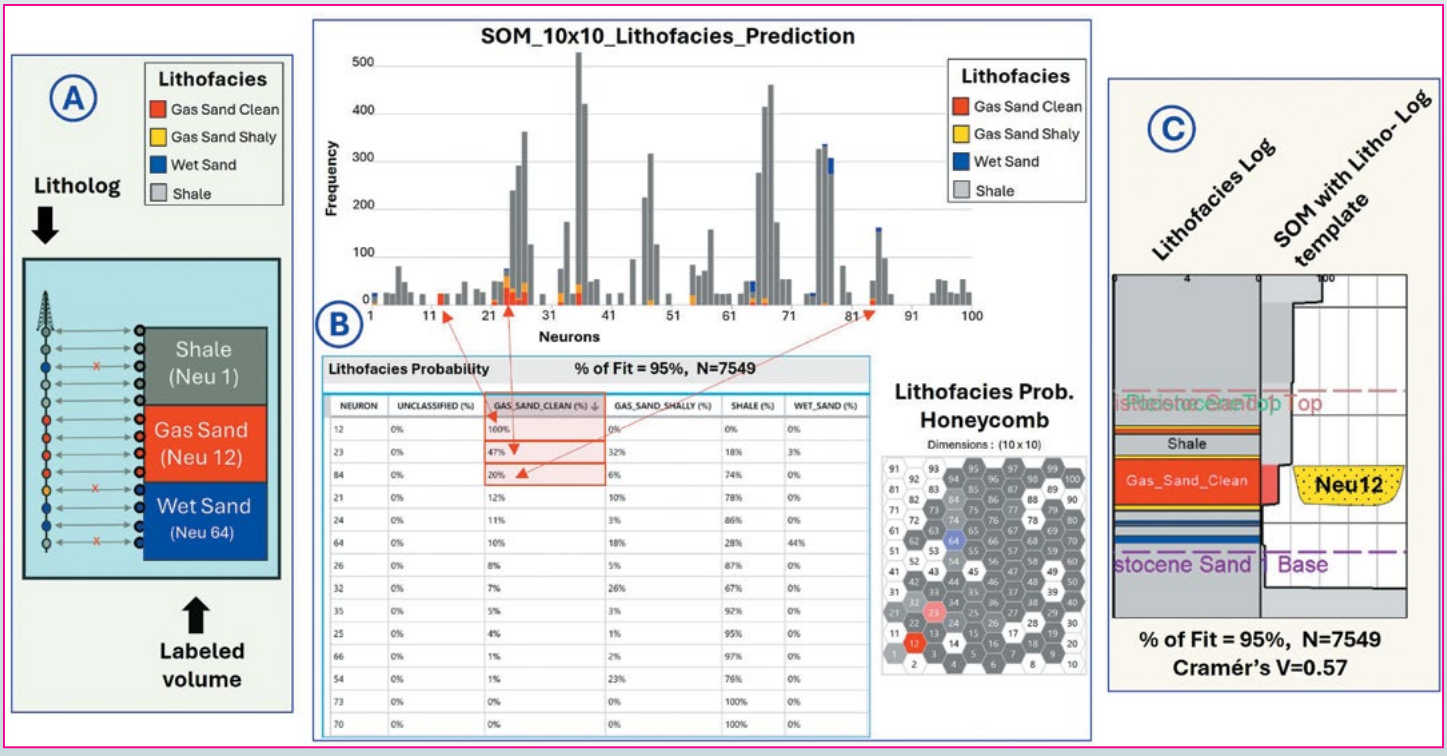

Figure 3. Lithofacies-to-SOM Process. A) Cartoon of the Lithofacies log versus SOM neuron cross tabulation. B) Stacked bars showing lithofacies log count by each SOM neuron, Contingency Table highlighting Gas Sand Clean Probability by neuron in descending order and Lithofacies Probability honeycomb. C) Actual comparison of Lithofacies log versus SOM with Litho-Log template in the well.

Continued on page 20

TABLE OF CONTENTS

the characteristics of reflectors (density, noise, dominant frequency, vertical shearing variation, dipping beds) and faults (dip, azimuth, location, displacements, attenuation, among others), allowing the algorithm to detect even the most 'imperceptible' faults to the naked eye (Qi et al, 2022). The workflow starts with a pre-conditioning step of the original seismic amplitude, using a Structure Oriented Filter (SOF3D) that involves the computation of Dip, Similarity and SOF3D volumes for suppressing noise. The CNN will perform the "computer vision" task of comparing the training data with the real filtered data and producing a set of fault attributes that include Fault Probability and Fault Classification. The next step is the post-processing of the fault images; creating more continuous features for faults (fault enhancement) and then sharpening them in the skeletonization process (Qi et al, 2020).

Results

In this study, we combined three key methodologies: K-means clustering for lithofacies classification from well logs, Self-Organizing Maps (SOM) for seismic multi-attribute classification at 4 milliseconds scale, and seismic fault detection using Convolutional Neural Networks (CNN) to build a high-resolution reservoir model.

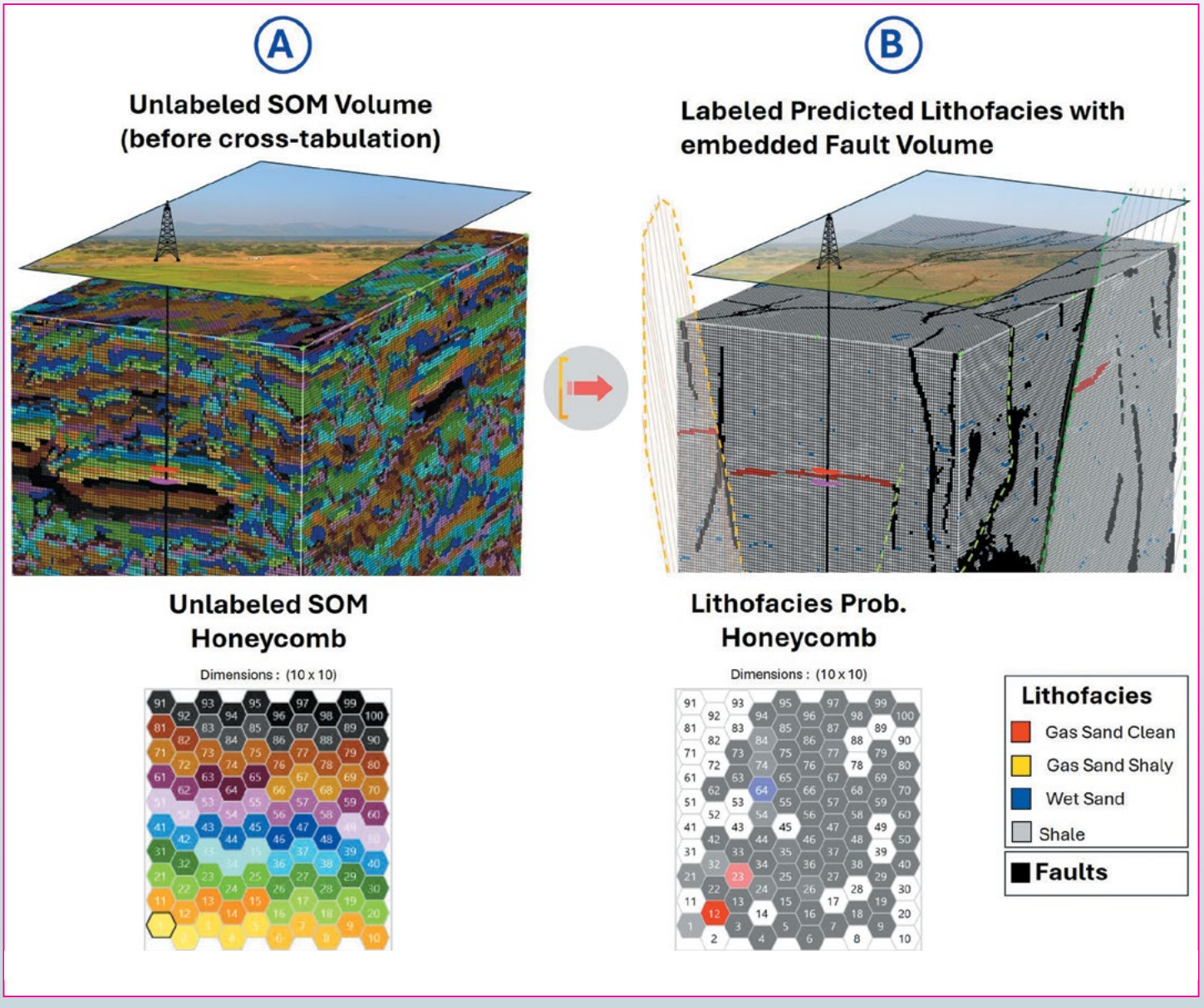

Figure 4. 3D Lithofacies Prediction (LP) volume. A) Unlabeled SOM classification Volume without 3D CNN faults. B) Predicted Lithofacies volume with embedded 3D CNN faults.

Continued on page 21

TABLE OF CONTENTS

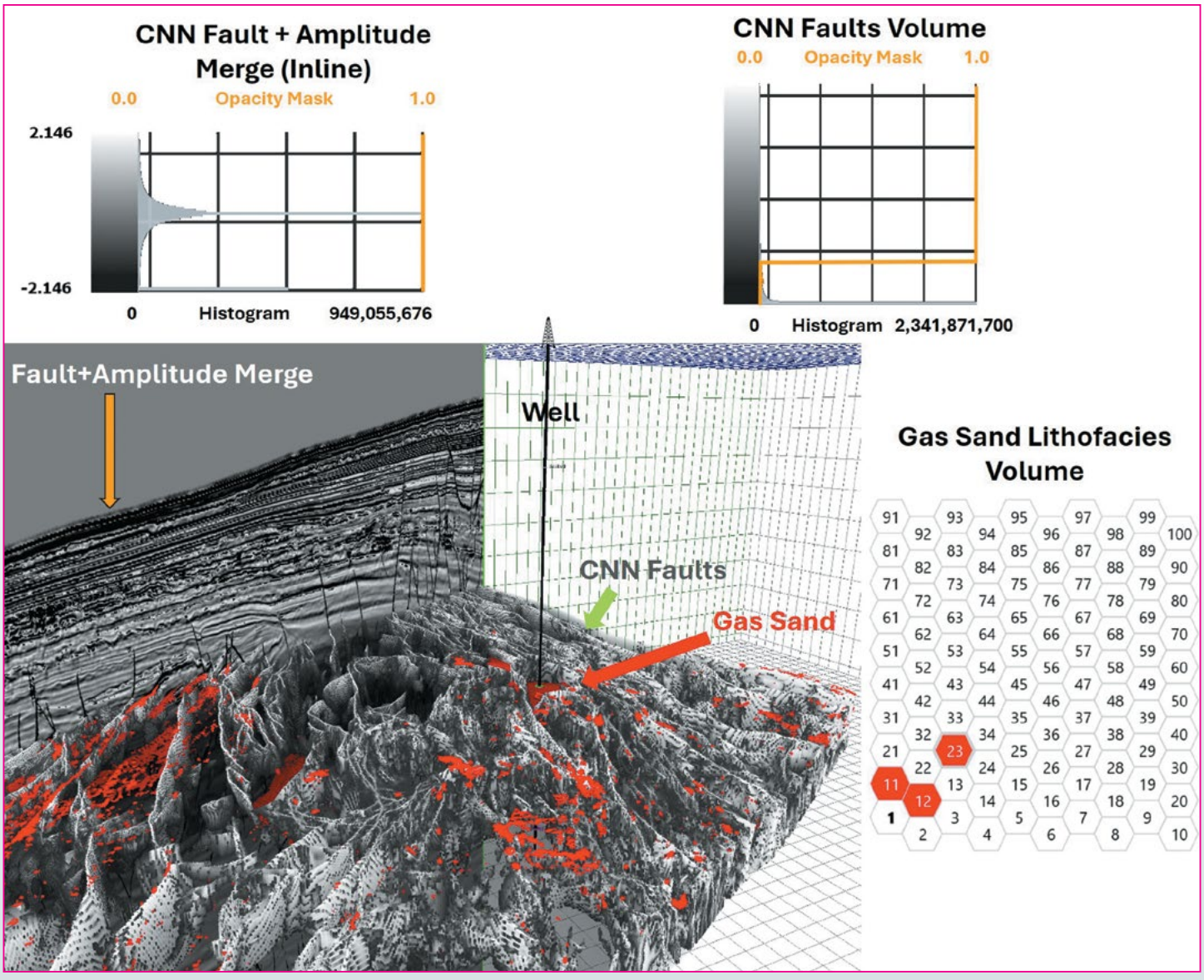

Figure 5. Perspective view of sculpted Gas Sand geobodies and CNN Faults showing detected structural compartments in the well vicinity and in new zones of interest.

We first applied K-means clustering to well log data, generating a lithofacies log based on effective porosity, water saturation, and shale volume. Four distinct clusters or lithofacies were identified in the histograms, reflecting their respective data distributions: Shale, Clean Gas Sand, Shaly Gas Sand, and Wet (Brine) Sand (Figure 2, corners). These clusters were subsequently used to create a lithofacies log for the well, where the most significant sandstone layer encountered measures only 5 meters in thickness (Figure 2, center). As illustrated in Figure 3, the lithofacies log provided the basis for extending facies classification across the seismic SOM volume. The sampling interval scale-based SOM multi-attribute seismic analysis enabled resolving the sandstone mentioned above. Each one of the SOM voxels (neurons) extracted along the well path was analyzed according to its lithofacies log, determining in a quantitively manner through contingency tables the probability of each neuron representing a specific lithofacies. With a total of 7549 samples evaluated, the percentage of fit between the lithofacies log and the predicted lithofacies volume is 95%. After grouping similar neurons in the contingency table, several parameters were computed to obtain Cramér's V equal to 0.57, with a predefined Type I error equal to 0.05, the Chi-square statistic of 2486.26, three degrees of freedom, p-value of 0 and Statistical Power of 0.96. All these statistical parameters provide evidence of a strong association between the seismic lithofacies prediction (LP) classification volume and the lithofacies log.

Continued on page 22

TABLE OF CONTENTS

Figure 4A shows the SOM volume before Lithofacies Prediction (LP), while Figure 4B, displays the LP volume with embedded 3D CNN faults.

Finally, Figure 5 presents a perspective view showcasing how the detected fault planes contributed to delineating structural compartments within the seismic volume. This integration offers a framework for lithofacies distribution and structural compartmentalization, which can support future updates to the geological model.

Discussion and Conclusions

The integration of lithofacies log classification, seismic multi-attribute analysis, and fault detection has significantly refined our understanding of the Rajahmundri Sandstone and Ravva Formation within the basin. By combining K-means clustering on well log data with Self-Organizing Maps (SOM) on seismic attributes, we created a high-resolution lithofacies model that aligns well with the depositional complexity and structural heterogeneity of the basin.

K-means clustering allowed us to define lithofacies based on porosity, shale volume, and water saturation, providing a direct, interpretable lithofacies log to guide reservoir characterization. This approach is particularly valuable given the stratigraphic unit thin sandstone layers. Importantly, the powerful SOM's sampling interval multi-attribute classification extended lithofacies beyond the well, capturing seismic responses of each lithofacies at a fine spatial scale. This integration is crucial in complex environments where conventional seismic alone might not sufficiently differentiate between lithofacies.

The fault detection using CNN-based seismic analysis added another layer of precision, defining structural compartments and enhancing the lithofacies model's accuracy. Fault planes, mapped directly into the Gas Sand and Shale lithofacies volumes, revealed structural entrapment mechanisms essential for understanding reservoir connectivity. This integrated approach not only refines the interpretation of reservoir architecture but also streamlines the interpreter's workflow by bringing together essential elements in a unified model, allowing for a comprehensive view of lithofacies distribution and structural compartmentalization.

By incorporating faults within lithofacies distributions, the model provides a robust framework for geologic continuity and compartmentalization, aligning with observed growth fault systems and toe-thrusts from previous basin studies. This combined approach ultimately delivers a more accurate reservoir model that can drive future exploration and development strategies in the basin by addressing both stratigraphic and structural elements in an integrated, data-driven manner.

Congratulations to Craig

Craig Beasley played a pivotal role in the founding of Geoscientists Without Borders (GWB). His ongoing dedication has been crucial in ensuring that GWB consistently fulfills its mission: leveraging geosciences to address humanitarian challenges and fostering the next generation of geoscientists through active student participation in projects.

SEG FOUNDATION

GEOSCIENTISTS without BORDERS®
SOCIETY OF EXPLORATION GEOPHYSICISTS

Acknowledgments

The authors wish to express their gratitude to Hal Green and Geophysical Insights for providing access to the Paradise software and extend their thanks to our client for granting permission to publish the paper.

References

i. Avseth, P., Mukerji, T., and G. Mavko, 2005, Quantitative Seismic Interpretation. Applying Rock Physics Tools to Reduce Interpretation Risk: Cambridge Univ. Press.

ii. Chaveste, A., Roden, R., and T. Smith, 2023, Machine Learning-Based Method Provides Economic Option To Seismic Inversions: The American Oil & Gas Report, 66, no. 11.

iii. Harikrishna, S., Jagannadha Rao, M., Asha, V., Swathi, G., and G.N. Rao, 2023, Paleo-Depositional Systems in the Krishna Godavari Basin, East Coast of India: Tuijin Jishu/Journal of Propulsion Technology, 44, no. 4, ISSN: 1001-4055.

iv. Gupta, S. K., 2006, Basin architecture and petroleum system of Krishna Godavari Basin, east coast of India: The Leading Edge, 25, no. 7.

v. Indian Plate Lexicon of Stratigraphic Units, 2024, Cenozoic of Eastern Indian Basins, On-line search in: https://indplex.geolex.org/wells/Cenozoic_Eastern_Basins.php.

vi. Kohonen, T., 1982, Self-organized formation of topologically correct feature maps: Biological Cybernetics, 43, 59–69.

vii. Mavko, G., Mukerji, T., and J. Dvorkin, 2009, The Rock Physics Handbook, Second Edition Tools for Seismic Analysis of Porous Media: Cambridge Univ. Press.

viii. Smith, T., and S. Treitel, 2015, Self-Organizing Neural Nets for Automatic Anomaly Identification, A white paper, https://www.geoinsights.com/self-organizing-neural-nets-for-automatic-anomaly-identification/Npdf-13.

ix. Qi, J., Lyu, B., Wu, X., and K. J. Marfurt, 2020, Comparing convolutional neural networking and image processing seismic fault detection methods: 90th Annual International Meeting, SEG, Expanded Abstracts, 1111–1115, https://doi.org/10.1190/segam2020-3428171.1.

x. Qi, J., Laudon, C., and K.J. Marfurt, 2022, An integrated machine learning-based fault classification workflow: Second International Meeting for Applied Geoscience & Energy, SEG/AAPG, Expanded Abstracts, 1865–1869.

xi. Wu, X., Shi, Y., Fomel, S., Liang, L., Zhang, Q., and A. Z. Yusifov, 2019, FaultNet3D: Predicting Fault Probabilities, Strikes, and Dips With a Single Convolutional Neural Network: IEEE Transactions on Geoscience and Remote Sensing, 57, no. 11, pp. 9138–9155, Nov. 2019, doi: 10.1109/TGRS.2019.2925003.

TABLE OF CONTENTS

Introduction to A More General Refraction Theory

Chuck Diggins, Down Under GeoSolutions

Abstract

Conventional refraction analysis incorrectly associates seismic first breaks purely with refractors. However, first break times are a combination of shallow anomalies imprinted on refracted arrivals. As a result, first breaks produce inaccurate tomographic models and statics. These flawed models are being used as the near-surface components for PSDM and for initial FWI models.

This paper introduces "A More General Refraction Theory" or AMGRT. AMGRT assumes that first-break picks consist of two separate components: a superficial, short-wavelength, surface-consistent component and a deeper, long-wavelength refracting component. We show, using seismic data from the Anadarko Basin, how the components are separated. Shot and receiver statics are derived from the superficial component and long-wavelength statics are computed from a tomographic model constructed from the refracted component. Statics from both components are added. These data are then stacked, demonstrating the efficacy of AMGRT.

Conventional Refraction Statics

In land seismic processing two classes of refraction algorithms are typically used for computing refraction statics: First, a delay-time solution, where one or more separate refractors can be analyzed and their results combined into an earth model comprising discrete layers. Alternatively, a turning-ray tomography solution, where first breaks from near to far offsets are analyzed to construct a continuous velocity model which best fits the arrivals. In practice, both algorithms are widely used. In fact, for any given production dataset, both approaches are often attempted with the better of the two solutions determined by stack response to be carried forward into production processing. Delay-time statics have been used almost since multi-channel seismic data has been acquired. Cox (1999) describes the historical use of first breaks for computing statics. Delay-time statics have been described in many papers, including Diggins, et al (1988), Palmer (1980). Tomographic statics have also been described in many papers, including Epili, et all (2001) and Zhu, et al (1992).

The problem is both classes of conventional refraction-based algorithms see first breaks as refracting events generated in the near-surface. Figure 1 shows a representative near-surface model with a gradient of increasing velocities starting at surface topography. Refraction tomographic algorithms generate turning-ray

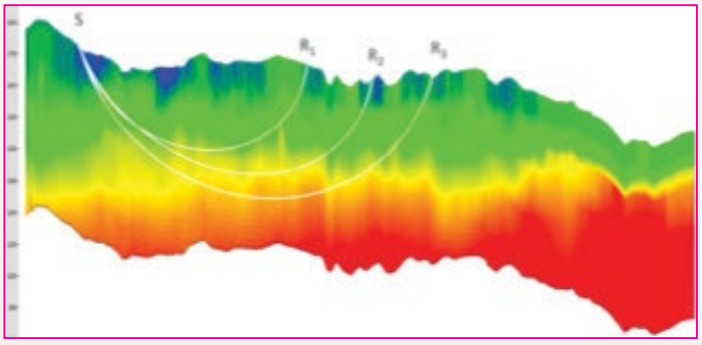

Figure 1. Cross-section of a turning-ray tomography model from the Anadarko Basin used in this paper. Hypothetical turning-ray paths are shown from a shot at S to three receivers at R. Tomography models show a continuous velocity gradient from the surface.

paths through this model starting and ending at the surface as shown for the shot S into receivers R. Tomographic models have been used extensively for many years to compute statics.

The True Nature of First Breaks

The conventional view of first breaks is not correct. In AMGRT, first breaks are seen as a combination of non-

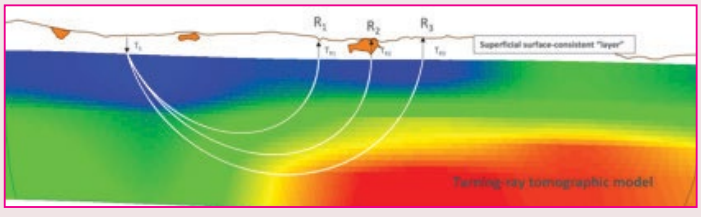

Figure 1. Conceptual near-surface model used by AMGRT showing shallow, surface-consistent component above and the deeper turning ray component below.

Continued on page 27

TABLE OF CONTENTS

refracted and refracted components. The non-refracted component is generated at the very near-surface and is thus surface-consistent. In fact, surface-consistency itself implies anomalies must be at or very near the surface. Daly, et al (1988) alluded to this behavior.

The refracted component is generated by the deeper seismic wavefield. Figure 2 shows a model with a shallow layer with vertical travel paths in the shallowest layers and turning rays in the deeper model characterized by a velocity gradient. This model is reminiscent of the near-surface model envisioned for reflection-based statics in Wiggins, et al (1976).

A More General Refraction Theory (AMGRT)

AMGRT recognizes first breaks are composed of two distinct components: a shallow component and a deep component. This is expressed in the AMGRT pick time equation,

$$t(x) = t_x + \tau(x) + t_r$$

Where $\tau(x)$ is the long-wavelength refraction time at offset, x. The short-wavelength surface-consistent source and receiver statics are t_x and t_r. Figure 3 shows this

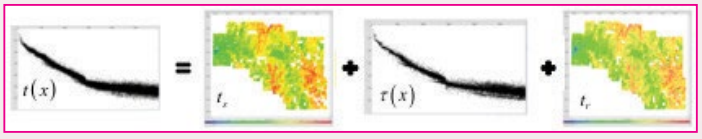

Figure 3. AMGRT pick time decomposition expressed graphically. Note how the $\tau(x)$ term above shows the linear refracted events more clearly than the input picks $t(x)$. This is because the superficial statics terms t_x and t_r have been removed.

equation graphically after the input first break pick times $t(x)$ were decomposed into t_x, $\tau(x)$ and t_r, respectively. The $\tau(x)$ term will be used to construct a "sanitized" tomographic model. This model will have none of the surface-consistent statics embedded in the picks and thus will result in a more accurate near-surface long-wavelength model than conventional the conventional approach. This is shown in Figure 4. Figure 4 demonstrates that AMGRT on the right does not have the imprint from surface-consistent components, since they have been removed.

Figure 5 shows a stack QC comparison between conventional tomographic statics and AMGRT statics. The AMGRT statics are the sum of the superficial statics, t_x and t_r plus the statics computed from the AMGRT-derived tomographic model shown on the right in Figure 4.

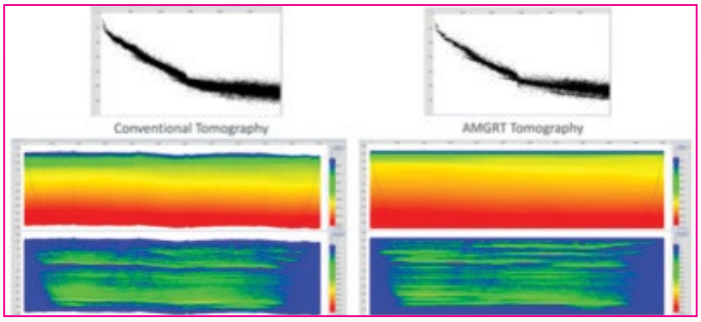

Figure 4. Conventional tomographic model (left) versus AMGRT-derived tomographic model (right)

Figure 6 shows 2 stacks, one without statics (left) and the second (right) with only the superficial shot and receiver statics (t_x and t_r) applied. Most of the AMGRT-derived statics that were applied in Figure 5 are in fact

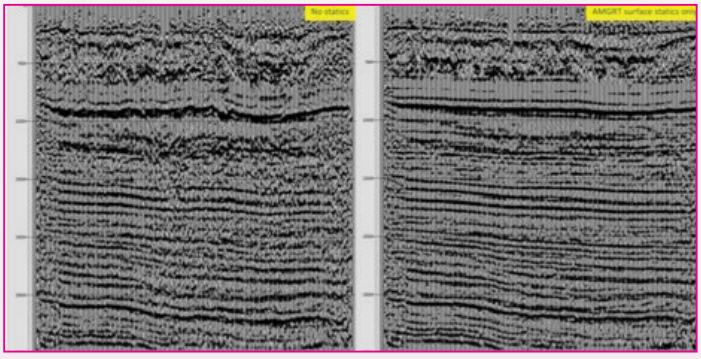

Figure 5. Stack comparison between conventional tomographic statics (left) and AMGRT statics (right)

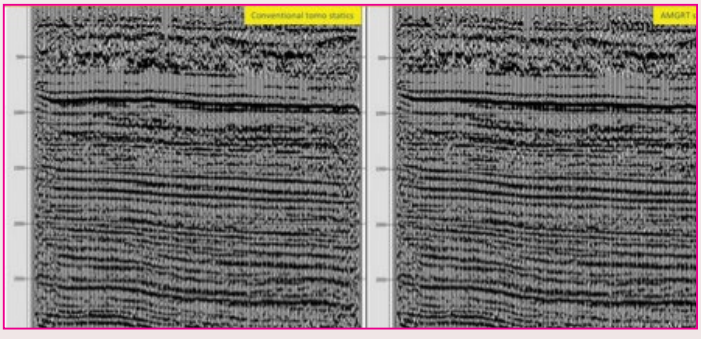

Figure 6. Stack comparison between no statics (left) and AMGRT surface statics only. No tomographic statics were applied.

the superficial statics! The AMGRT-derived tomographic model only contributes to the long-wavelengths.

Continued on page 28

TABLE OF CONTENTS

Conclusion:

AMGRT recognizes that first breaks are composed of a combination superficial surface-consistent short-wavelength statics and deeper long-wavelength refracted arrivals. By decomposing the first breaks into surface-consistent statics and long-wavelength refracted arrivals, AMGRT generates better surface-consistent statics and more accurate tomographic near-surface models. Indeed, we have found that the surface consistent statics derived using AMGRT are both easier to generate and better in quality than traditional automatic residual statics derived from reflection events.

AMGRT's statics improve both time and depth processing, including preparing seismic data prior to FWI. AMGRT's tomographic models will provide more accurate near-surface models for PSDM and improved initial near-surface models for FWI.

Acknowledgments

We would like to thank Fairfield Geotechnologies for their use of the Caddo survey from the Anadarko Basin, especially Bruce Karr (Fairfield) for his comments and suggestions.

References

i. Cox. M, 1999, "Static Corrections for Seismic Reflection Surveys".

ii. Daly, C, and Diggins, C., 1988, The use of refraction elevation models in the computation of statics, 50th EAGE Annual Meeting.

iii. Diggins, C, Carvill, C and Daly, C., 1988, A hybrid refraction algorithm, 58th Annual International Meeting, *SEG Technical Program Expanded Abstracts* : 578-581.

iv. Epili, D, Criss, J, Cunningham, D, 2001, Turning-Ray Tomography For Statics Solution. 2001 SEG Annual Meeting, San Antonio, Texas

v. Palmer, D, 1980, The Generalized Reciprocal Method of Refraction Interpretation, SEG.

vi. Hawkins, L. V., The reciprocal method of routine shallow seismic refraction investigations: Geophysics, v. 26, p. 806-819.

vii. Wiggins, R. A., Larner, K. L, and Wisecup, R. D., 1976, Residua static analysis as a general linear inversion problem,: Geophysics 41: 922-938.

viii. Zhu, X., Sixta, D. and Angstman, B, 1992, Tomostatics: Turning-ray tomography + static corrections, *The Leading Edge 11*: No 12, 15-23.

Case Study Academy One Day Seminar featuring Exploration Success Stories and Comebacks from Dry Holes

By: Linda Sternbach, Charles Sternbach, and Katya Casey.

In November, GSH and Houston Geological Society teamed up to present "Case Study Academy: Lessons from Missed Opportunities and Surprise Successes" co-hosted by Katya Casey (GSH Honorary Member) and Charles Sternbach (HGS and AAPG Honorary Member). Speakers shared their trial-and-error paths, perseverance, and navigation of the corporate decision-making process for sound investment in the uncertain world of subsurface characterization. This unique event was designed as an interactive training experience to expose participants to integrated case studies and stimulate professional discussion, geologic model testing, and networking for geoscientists of all ages and backgrounds. 140 participants, including 17 geoscience students, participated in panel discussions, asked questions, and made valuable professional connections.

TABLE OF CONTENTS

Doodlebugger Diary

'Telseis' System Eliminates Use of Cables in Difficult Areas

Story by Western Geophysical Area Manager J. P. Denniston • Photos by Western Geophysical Party 101 Manager Victor Courtice • Originally published in the 1975 Spring - Summer Western Profile • Recounted by Scott Singleton

The Doodlebugger Diary recounts the experiences of geophysicists during their working lives. I've published extensively on my own experiences and encourage those of you with experiences of your own to also contribute. Your fellow industry professionals would love to hear your stories.

Previously I reprinted a series of early 1980's articles from the GSI Shotpoints and GSI Grapevine that can be found at http://gsinet.us/. However, in the past few years I have been reprinting various interesting and engaging Western Geophysical Profile articles from the 1970's, which is interesting to me because this is when I first became a doodlebugger and is the company that first hired me to work offshore. The full set of scanned Profile issues can be found at https://library.seg.org/page/western-profile.

Prolog by Scott Singleton

Nowadays, ocean bottom nodes (OBN) are ubiquitous in the seismic acquisition industry, and in fact some would claim they are the preferred means of acquisition due to the lack of ghosting problems in the water column. But as you might well imagine, they have not always been so. It is only with technological advancements that receivers became usable in deep water and communications became reliable between receiver and acquisition vessel. Thus, this month's Doodlebugger Diaries explores the development of one of the precursors to this methodology via the use of radio telemetry systems in shallow water transition zone surveys.

During the 1970's, several companies were developing radio telemetry for use in various challenging acquisition environments. Among these were GSI, Western Geophysical, Geco-Prakla, and Digicon. However, RF systems stayed as a niche technology because of the onset of ocean bottom cables (OBC) which were easier to use and didn't have the RF issues (these were on cables that were connected directly to the recording boat, much as streamers were).

But for transition zone surveys, RF systems easily became the go-to technology to use, at the time bridging the gap between land surveys and shallow water OBC or streamer. Our present article from the Western Profile in 1975 describes the first use of an RF technology they called 'Telseis' which was a big deal back then.

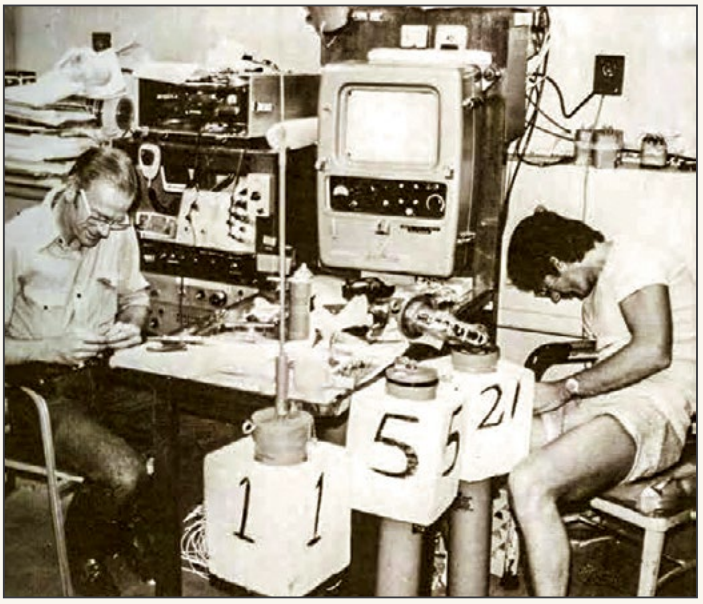

Figure 1: *Party 101 radio technicians assemble Telseis buoys and attach flotation collars.*

Continued on page 31

TABLE OF CONTENTS

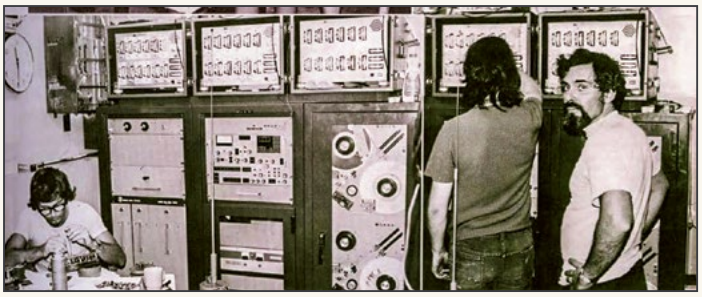

Figure 2: *Party 101 instrument technicians at work in the recording room of the Western Beach. The lower rack contains the DDS 888 recording system with IBM 3480 tape drives. The Telseis instruments are in the upper rack.*

Figure 3: *The Rotork "Tork 2" utility boat is lifted aboard the Western Beach to join "Tork 1," which is already on the helideck.*

However, my follow-up search to figure out how successful the technology was and where it was used after the initial survey did not bear any fruit. Instead, what I found was repeated references to a company called Fairfield Industries being formed in 1976 and immediately using what they called the Telseis system (which they copyrighted) on 2D transition zone surveys in Louisiana. This later became known as the Telseis Star system (again, copyrighted).

So I began to look into this new company and its use of this technology. Apparently, Fairfield Industries changed its name in 2010 to FairfieldNodal, acknowledging the fact that they were mainly an OBN company that had developed its own cableless equipment which they called ZNodal. This is broken into ZLand and ZMarine (which they were stretching into progressively deeper water). Then in 2018 they acquired WGP and Geokinetics' multiclient data library, renamed themselves as Fairfield Geotechnologies, and then late that year sold all their technology to Norway's Magseis, thus becoming primarily a data processing and multiclient library company.

Mob and first use of the Telseis system onboard the Western Beach

Obtaining seismic information can be very difficult in certain kinds of terrain and waters, but there is a system to help overcome some of the difficulties: the Telseis RF telemetry system. It is designed to operate on radio frequencies from 30 to 76 megacycles with seismic signals from sensor arrays transmitted to onboard recording instruments. Highly mobile and flexible, it was used with much success in shallow water offshore Iran by Party 101 starting in June 1975 after being mobilized onto the M/V Western Beach in Bahrain in the spring of 1975. (Ed note: the photos in this article are from that mob).

Useful in deep or shallow water using hydrophones, or on land using velocity phones, the system eliminates the normal use of seismic cables. In general the basic system is composed of a selected number of transceivers (buoys), each with a different designated radio frequency within the above range (Figure 1). One of these transceivers coupled with a string of detectors serves the same purpose as a 'group' on a normal cable; this in turn eliminates the handling of cables in difficult areas. An equivalent number of receivers on the recording boat is used to accept the signals and with these interfaced to a normal set of seismic recording instruments

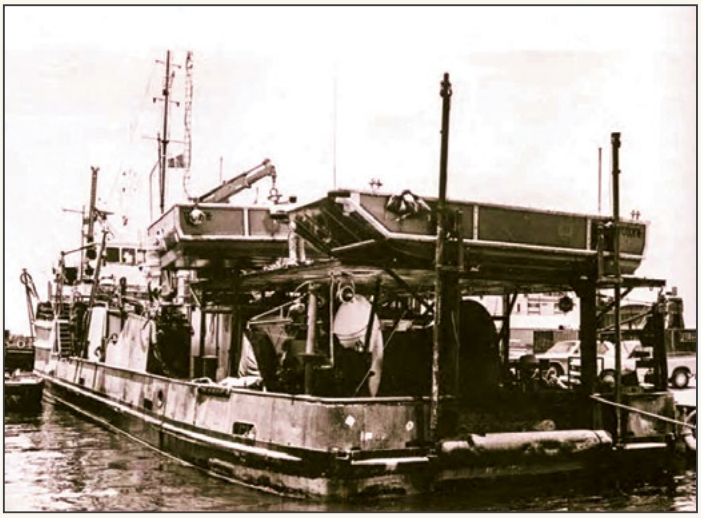

Figure 4: *The second Rotork being placed on the helideck.*

Continued on page 32

TABLE OF CONTENTS

with the data being recorded on magnetic tape (Figure 2). Information picked up by the sensor array is transmitted not through cable but by the buoys through the air as frequency modulated VHF radio signals.

An average operation using the Telseis system would utilize 36 transceivers in a roll-along sequence recording 24 channels of data at each shot location. The buoys are small enough that they can be set at the pre-located point using a small shallow-draft boat, yet the transmitters are capable of ranges of up to 20 miles, which allows the recording vessel to stay in deeper, safer water.
Party 101 has been using the Telseis system to great

Figure 5: *Party 101 crew prepare the Seiga to be lifted out of the water.*

advantage in the 'gray' area between deep water (25 feet) and shore. In the past it has been difficult to obtain coverage of this area. The first few months of Party 101's operation, however, indicate that this approach not only does allow the coverage but also obtains data of high quality.

Support equipment for Party 101's operation includes a mother ship, the Western Beach. The Beach could be considered a floating hotel and workshop, for that is

Figure 6: *The Seiga being lifted onto the helideck.*

where the crew returns each night to repair and service equipment and to sleep.

Work vessels are two shallow-draft boats, two rubber rafts, and an amphibious Seiga transport unit (described below) with a shallow utility vessel and a hovercraft available as needed. The 9-foot-wide, 25-foot-long, shallow-draft boats are Rotorks called Tork I and Tork II (Ed note: A Rotork Sea Truck is a flat-bottomed, fiberglass, high-speed watercraft, similar to a small landing craft. They are used to land vehicles in areas without jetties or harbor facilities) (Figures 3 and 4). Powered by Volvo Penta 106-horsepower engines; one is used as a navigation or survey vessel and the second as a shooting boat.

The two inflatable rubber rafts, called Zodiacs, are used to lay out and pick up the buoys. The additional boat and the hovercraft can also be used to handle the buoys. With most of the program designed to extend onto land, a transport vehicle was needed - the amphibious Seiga (Figures 5 and 6). This is a simply designed vehicle capable of operating in very shallow water as well as on land by the use of large tires that have paddle-like treads (Figure 6). The hovercraft is also a big asset to this phase of the operation.

The set-up and operation are comparable to a land roll-along operation, with small boats used in lieu of trucks, the Telseis buoys in place of cables, and the recording boat instead of a recording truck.

Everyone at Western Geophysical is looking forward to this new and innovative transition zone operation system to enhance our capabilities in providing a unified, consistent seismic image from land into deep water.

Corporate Members

TABLE OF CONTENTS

New Algorithms to Fully Automate 3D Seismic Data Interpretation

Norman Mark, October 28th, 2024

Introduction

This article is an extension of my work appearing in this publication about 2 years ago which presented automating horizon picking from 2D seismic data. After accomplishing that I had a long-enduring mental block on how to extend the method to 3D for the purposes of automating subsurface mapping, the most tedious, time-consuming, error-prone and least appreciated processes in all of oil and gas exploration, and arguably the most important: no map, no drilling! Bad map – dry hole (usually). Good map – production (maybe). Maps based on artistic inclinations or sales purposes rather than strictly honoring data have led to legendary O&G financial failures.

Here I present the output of code I wrote which actually does automate 3D seismic interpretation, fully honoring all the data, to your profound disbelief, I suspect – and without any wishful-thinking component built in to the computing.

My decades-long experience working with oil and gas exploration and seismic service companies gave me the foundation and curiosity for pursuing the goal of automating seismic survey data mapping and immunized me against self-punishment.

The input data used here are from a good quality public domain 3D seismic data volume, Parihaka, offshore New Zealand, and are pushed through my code on a 10-year old Intel(R) Core(TM) i7-5600U CPU @ 2.60GHz laptop. As it has no graphics card I tested it for graphics capacity to learn how much data it could handle in case I got lucky with my code. Surprisingly, the upper limit for drawing a 3D random point cloud in a browser is 30 million points with about 5 minutes of waiting for the blank browser window to light up with points.

Data Selection

An arbitrary data prism of 101 inlines x 101 crosslines - 10201 traces containing 2 seconds of better than average seismic reflection data quality from the Parihaka cube. The sample rate is 3ms. From this sub-volume local maxima reflection times were computed and used in this study. No filters of any kind were applied to these input data. This 101 traces x 101 traces x 2 seconds data prism contains almost 1 million/over 940,000 peak reflection times. Figure 1 contains views of the data at 3 different depth ranges within my 3D viewer. On the right the full volume of reflection points is colored by depth.

Much can be learned about the geologic structure from these views of the data alone without any further computing beyond computing local maxima from SEGY

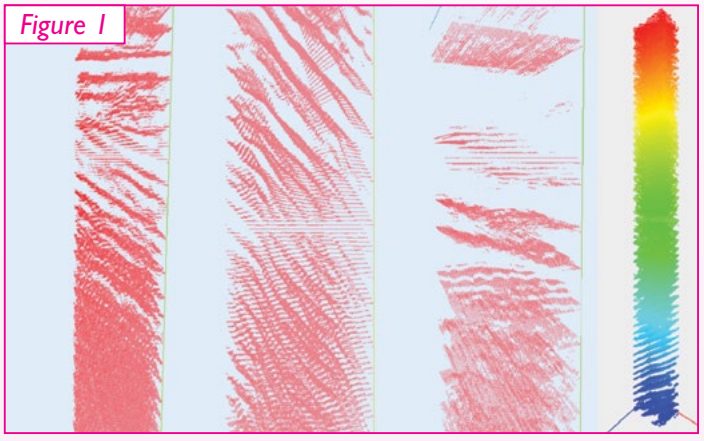

Figure 1

data. This style of data viewing has not been available in the commercial seismic interpretation software I have seen. The 3D viewer makes it easy to quickly identify zones of interest/targets especially with its transparency options. Again, these data are raw peak times – no amplitude information or isolation of surfaces.

Work Flow

The first step in finding surfaces is finding 2D horizons within each of the separate seismic inlines. Horizons are defined by touching 2D points within an inline or x-plane. By touching, I mean x coordinates change by one and y coordinates change by zero or one.

The following images, Figure 2, show the results of this process. Red points are local maxima and the green lines are the horizons. The left side shows a trace-long

Continued on page 35

TABLE OF CONTENTS

section of an inline with 2 seconds peak reflections. The right side is a detailed view of horizons indicated by their connectivity. Green lines connect reflection points one separated by one crossline, typically 12.5 to 25 meters in a modern seismic survey.

Figure 2

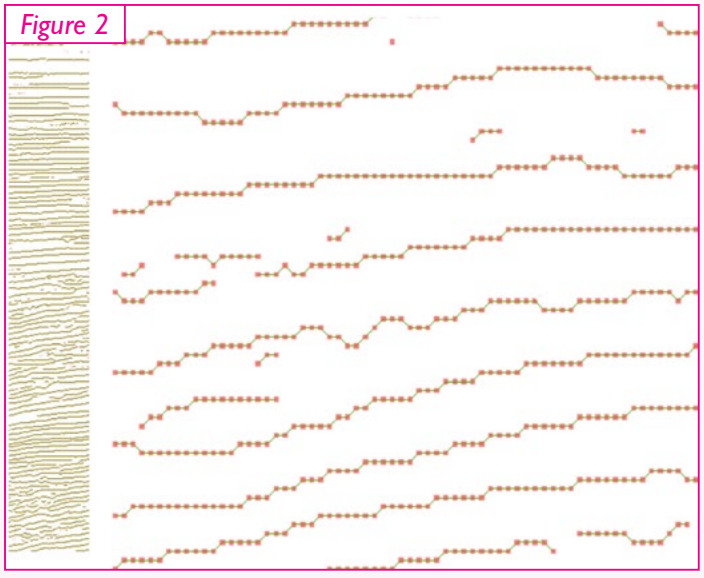

The three images in Figure 3 show views of the entire data volume of touching – one unit separation - positive reflection points connected by lines.

Figure 3

These entire volume of chains of points are computed in less than 4 minutes and are output to a text file in the following x,y,z format style:

1837,-92,4240 -> 1837,-93,4241
1837,-92,4244 -> 1837,-92,4245 -> 1837,-92,4246 -> 1837,-93,4247
1837,-92,4251 -> 1837,-92,4252 -> 1837,-92,4253 -> 1837,-92,4254 -> 1837,-92,4255
1837,-92,4257 -> 1837,-92,4258 -> 1837,-92,4259 -> 1837,-92,4260 -> 1837,-92,4261 -> 1837,-92,4262 -> 1837,-92,4263 -> 1837,-93,4264

Here, 4 chains of 3D points – 4 horizons – are shown in inline, reflection time, and crossline with connections between points indicated by arrows. Time is negative in order to display reflection time increasing downward within my 3D viewer.

Although surfaces composed of touching reflection points are seen in these images, the 2D horizons have not been organized into surfaces yet. The chains of points are the input to my algorithm which computes the 3D surfaces. My definition of a surface for this purpose is an assembly of touching points one point thick completely surrounded by open space.

I built 3D viewers to display the input data and 3D surfaces using ThreeJS. Surfaces larger that 5000 points, out of a possible 10,201 points are shown in the below image, Figure 4. The surfaces were computed in about 15 minutes and are shown with unique colors to certify they are in fact entities.

Figure 4

The red axis indicates inline direction and the blue axis indicates crossline direction. The green y axis shows increasing reflection time downward, 0 to 2 seconds.

In another viewer, Figure 5, surfaces are colored by depth to show structural details.

Figure 5

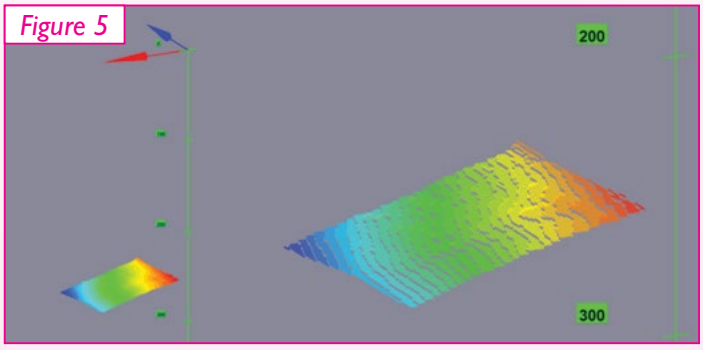

The output format for the surfaces is nearly identical to the format for the 2D horizons, except that the crossline (z-direction) values vary, as one would expect with surfaces. The output file is a listing of touching/adjacent 2D horizons in text format, easily read by mapping software which reads ASCII files.

Computing hundreds of surfaces took twenty minutes of computing on my 10-year old laptop. Mapping these same surfaces using O&G exploration commercial mapping software would take months!

I am currently seeking to apply my software to interested parties.

TABLE OF CONTENTS

Tutorial on Displaying 3D Data

By: Norman Mark

The image below is a screen shot of the HTML page which follows. All the images in this paper are from html pages using ThreeJS and JavaScript. ThreeJS is a JavaScript library of WebGL functions to which everyone has access. There is no need to download a language or install an IDE to be able to create a 3D image in a web page very quickly.

The HTML page which follows the image contains many comments about the purposes of the JavaScript syntax, but not everything is commented. However, one only needs limited fluency in HTML and JS to get a movable image onscreen quickly.

threejs.org is the dedicated website with many breathtaking examples of 3D graphics. It sold me! The views of seismic data I created in this article are trivial compared to what can be done in ThreeJS. Learning its full capability takes long and the online manual is cryptic. Further, tedious searching is most often necessary to understand a particular function parameter. Some are straightforward though.

Copy and paste the text below the image into a text editor and name the file with an html suffix, load the file into a browser (I use Firefox) and you will have the below image on your screen and be able to move the data volume and see point coordinates by clicking on them. Give your input data file a name with a txt suffix. The file should contain point format txt as in x1,y1,z1 x 2 , y 2 , z 2 , x3,y3,z3…

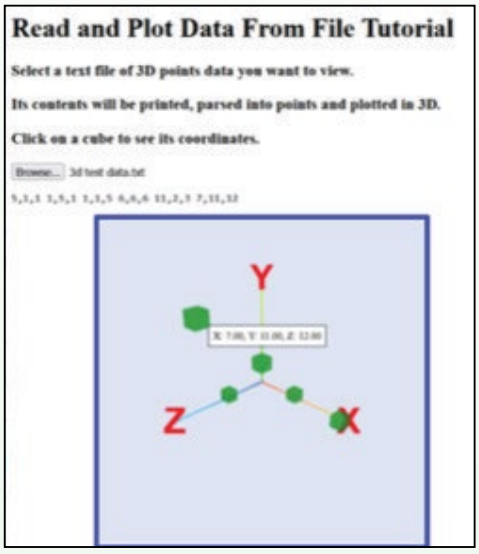


```
<!DOCTYPE html>
<html>
<head>
    <title>Read Text File and 3D Viewer</title>
    <h1> Read and Plot Data From File Tutorial </h1>
    <h3> Select a text file of 3D points data you want to view.</h3>
    <h3>Its contents will be printed, parsed into points and plotted in 3D.
    </h3>
    <h3>Click on a cube to see its coordinates.</h3>
    <style>
        /* Set viewer dimensions and border */
        #viewer {
            width: 400px;
            height: 400px;
            margin-left: 100px;
            margin-bottom: 200px;
            border: 5px solid blue;
            position: absolute;
            box-sizing: border-box;
        }
    </style>
</head>
```

Continued on page 37

TABLE OF CONTENTS

```
<body>
    <input type="file" name="inputfile" id="inputfile" text="input">
    <br>
    <pre id="output"></pre> <!-- this is where the input text is printed after
       being parsed into points for QC purposes -->
    <div id="viewer"></div>
    <div id="tooltip" style="position: absolute; display: none; background:
       white; border: 1px solid black; padding: 5px; font-size: 12px;
       pointer-events: none;">
    </div>

    <script type="module">
        import * as THREE from ,https://threejs.org/build/three.module.js';
        import { OrbitControls } from ,https://cdn.skypack.dev/three@0.132.2/
        examples/jsm/controls/OrbitControls.js';

        let scene, camera, renderer, controls;

        // Initialize the 3D scene
        function init() {
            scene = new THREE.Scene();
            renderer = new THREE.WebGLRenderer({ antialias: true });
            renderer.setSize(390,390);    // 10 less than the width and height
            //renderer.setSize(viewer.offsetWidth, viewer.offsetHeight);
            renderer.setClearColor(0xdde5ff); // Pale blue background color
            //html color picker at https://www.w3schools.com/colors/colors_
            picker.asp
        document.getElementById(,viewer').appendChild(renderer.domElement);

        const raycaster = new THREE.Raycaster();
        //raycaster.far = 20;
        raycaster.near = .5;
        raycaster.params.Points.threshold = 0.01; // Tolerance can be adjusted
        as needed
        const mouse = new THREE.Vector2();
        const tooltip = document.getElementById(,tooltip');
        renderer.domElement.addEventListener(,click', onMouseClick, false);

        // Camera setup
        camera = new THREE.PerspectiveCamera(45, viewer.offsetWidth / viewer.
        offsetHeight, 0.1, 1000);
        camera.updateProjectionMatrix();
        camera.position.set(40,30,40);
        camera.lookAt(scene.position);
        //camera.lookAt(0, 0, 0);

        // OrbitControls for rotation, zoom, and pan
        controls = new OrbitControls(camera, renderer.domElement);
```

Continued on page 38

TABLE OF CONTENTS

```
controls.enableDamping = true;
controls.dampingFactor = 0.1;
controls.enableZoom = true;
controls.enablePan = true;
controls.update();

// Axes helper
const axesHelper = new THREE.AxesHelper(10);
scene.add(axesHelper);

// Add light sources to the scene for shading
const ambientLight = new THREE.AmbientLight(0xa0a0a0); // Soft white
ambient light
scene.add(ambientLight);
const directionalLight = new THREE.DirectionalLight(0xffffff, 0.8);
directionalLight.position.set(15, 15, 15); // Position the light above
and to the side of the scene
scene.add(directionalLight);// required for shading cubes

// This section displays point coordinates on click
renderer.domElement.addEventListener(‚click’, onMouseClick, false);

function onMouseClick(event) {
      console.log(„Click detected at:”, event.clientX, event.clientY);
      const rect = renderer.domElement.getBoundingClientRect();
      mouse.x = ((event.clientX - rect.left) / rect.width) * 2 - 1;
      mouse.y = -((event.clientY - rect.top) / rect.height) * 2 + 1;
      raycaster.setFromCamera(mouse, camera);
      const intersects = raycaster.intersectObjects(scene.children,
      true);
      console.log(„Intersections:”, intersects);
if (intersects.length > 0) {
      const intersectedObject = intersects[0].object;
      if (intersectedObject.geometry && intersectedObject.geometry.type
      === ‚BoxGeometry’) {
      const position = intersectedObject.position;
      tooltip.style.left = `${event.clientX + 10}px`;
      tooltip.style.top = `${event.clientY + 10}px`;
      tooltip.style.display = ‚block’;
      tooltip.innerHTML = `X: ${position.x.toFixed(2)},
                           Y: ${position.y.toFixed(2)},
                           Z: ${position.z.toFixed(2)}`;
 }
} else {
 tooltip.style.display = ‚none’;
}
}
```

Continued on page 39

TABLE OF CONTENTS

```
// Optional: Hide tooltip on mouse move
renderer.domElement.addEventListener(,mousemove', () => {
      tooltip.style.display = ,none';
});

// Hide the tooltip when the mouse moves away or another point is clicked
renderer.domElement.addEventListener(,mousemove', () => {
      tooltip.style.display = ,none';
});

// Function to add sprite labels for each axis
function addSpriteLabel(text, x, y, z) {
   const canvas = document.createElement(,canvas');
   const context = canvas.getContext(,2d');
   canvas.width = 256;
   canvas.height = 256;
   context.font = ,Bold 75px Arial';
   context.fillStyle = ,rgba(255,0,0,1)'; // Red color for text
   context.textAlign = ,center';
   context.textBaseline = ,middle';
   context.fillText(text, canvas.width / 2, canvas.height / 2);
   const texture = new THREE.CanvasTexture(canvas);
   const spriteMaterial = new THREE.SpriteMaterial({ map: texture });
   const sprite = new THREE.Sprite(spriteMaterial);
   sprite.scale.set(10, 10, 1); // Make the text larger and more readable

// Set the sprite position
   sprite.position.set(x, y, z);
   scene.add(sprite);
}

// Call addSpriteLabel for each axis
   addSpriteLabel(,X', 10, 0, 0);  // Position near the end of the X axis
   addSpriteLabel(,Y', 0, 10, 0);  // Position near the end of the Y axis
   addSpriteLabel(,Z', 0, 0, 10);  // Position near the end of the Z axis

// Render the scene
animate();
}

// Animate the scene
function animate() {
   requestAnimationFrame(animate);
   controls.update();
   renderer.render(scene, camera);
}
```

Continued on page 40

TABLE OF CONTENTS

```
// Initialize the scene
 init();

// Parse the file's text into points and print the points in the console
 document.getElementById(,inputfile').addEventListener(,change', function()
 {
    const fr = new FileReader();
    fr.onload = function() {
        const data = fr.result.trim();
        const points = data.split(, ,).map(coord => {
            return coord.split(,,').map(Number);
        });

        // Print the points to the console
        console.log(points);

        // Display the raw data in the output element
        document.getElementById(,output').textContent = fr.result;

        // Add unit cubes at each parsed point
        points.forEach(point => {
            const cubeGeometry = new THREE.BoxGeometry(1, 1, 1);
            const cubeMaterial = new THREE.MeshStandardMaterial({ color:
             0x00ff00, transparent: true, opacity: .75 }); // for shaded sides
            const cube = new THREE.Mesh(cubeGeometry, cubeMaterial);
            cube.position.set(point[0], point[1], point[2]);
            scene.add(cube);
        });
      };
    fr.readAsText(this.files[0]);
  });
 </script>
</body>
```

Annual Sponsors

1790 W. Sam Houston Parkway N., Houston, TX 77043
Phone: (281) 741-1624 • Email: office@gshtx.org • Website: http://www.gshtx.org